Chapter 6

Cloverleaf Clusters: A Common Macrostructural Organization across Human Visual and Auditory Cortex

Alyssa A. Brewer and Brian Barton

Additional information is available at the end of the chapter

http://dx.doi.org/10.5772/intechopen.77964

Abstract

One of the fundamental properties of mammalian brains is that sensory regions of cortex are organized into multiple, functionally specialized cortical field maps (CFMs). An individual CFM is composed of two orthogonal topographical representations, reflecting two essential aspects of a sensory feature space. Each CFM is thought to subserve a specific computation or set of computations that underlie particular perceptual behaviors by enabling the comparison and combination of the information carried by the various specialized neuronal populations within this cortical region. Multiple adjacent CFMs, in turn, have now been shown by multiple laboratories to be organized in visual and auditory cortex into a macrostructural pattern called the cloverleaf cluster. CFMs within cloverleaf clusters tend to share properties such as receptive field distribution, cortical magnification, and processing specialization. This chapter will review the evidence for CFM and cloverleaf cluster organization across human visual and auditory cortex and will discuss the utility of these measurements for determining cortical structure and function and for investigating what changes occur in sensory cortex following various types of trauma or disease.

Keywords: visual field map, visual cortex, auditory field map, auditory cortex, cloverleaf cluster, cortical field map, cortical mapping, phase-encoded fMRI, population receptive field mapping

1. Introduction

Measurements in visual, auditory, and somatosensory cortices across numerous species of mammals have demonstrated that cortical field maps (CFMs) are a fundamental way for the brain

to represent sensory information [1–5]. CFMs arise from organized inputs from sensory organs (e.g., retina, cochlea, skin) that maintain the topographic organization of the sensory receptors in the cortex. Thus neurons whose sensory receptive fields are positioned next to one another in sensory feature space are located next to one another in cortex within a CFM. Knowledge of the properties of these CFMs is vital for understanding how specific sensory computations are processed across the brain. Basic stimulus features are processed in lower-level cortical regions, which then send information onto the next stage in the cortical hierarchy to undergo progressively more complex computations [6]. A common aspect of these sensory pathways is that the topography of the sensory receptors embodies the most fundamental stimulus information, which is conserved throughout most of the cortical hierarchy [7, 8].

A growing number of measurements in the visual and auditory systems have shown sensory CFMs to be organized into a macrostructural pattern called cloverleaf clusters, indicating that CFMs and cloverleaf clusters may both be fundamental organizing principles in cortical sensory processing [2, 4, 7–11]. Such organization may provide a basic framework for the complex processing and analysis of input from sensory receptors [12]. CFMs within clusters tend to share properties such as receptive field distribution, processing specialization, and cortical magnification (e.g., [10, 11, 13]). It is likely that this cluster organization, like the topographic organization of CFMs, allows for efficient connectivity among neurons that represent neighboring aspects in sensory feature space [14–17]. Since the axons contained within one cubic millimeter of cortex can extend 3–4 km in length, efficient connectivity is vital for sustainable energetics in cortex [18]. The cloverleaf cluster organization may thus be important for minimizing the length of axons connecting sensory maps within and between clusters, allowing for a more efficient ratio of brain matter to skull capacity.

The definition and characterization of CFMs and cloverleaf clusters have been indispensable in the investigation of the structure and function of human cortex, as these *in vivo* measurements allow for the systematic exploration of computations across a particular sensory cortex (for reviews, see [8, 12]). In addition, they can serve as excellent and dependable independent localizers for investigations of particular functions across individuals (e.g., [3, 4, 10, 13, 19, 20]). Thus, measuring the organization of individual CFMs helps elucidate the stages of distinct sensory processing pathways and can be used to track how the cortex changes under various disorders [21–28]. This chapter will review our current knowledge of the CFM and cloverleaf cluster organization across human visual and auditory cortex.

2. Techniques for measuring cortical field maps and cloverleaf clusters

2.1. Phase-encoded fMRI paradigms are used for measuring visual and auditory field maps

Obtaining a high quality measurement of topographic responses is the first step in accurately defining CFMs and requires choosing a set of stimuli that is appropriate for the sensory domain of interest. A highly accurate and powerful paradigm for measuring human CFMs *in vivo* relies on phase-encoded fMRI measurements (also known as "traveling wave"

measurements; **1**) [3, 4, 7, 29–32]. This technique uses two sets of periodic stimuli that each contain a set of stimulus values presented in an orderly sequence across a range of interest at a given frequency per scan (typically 6–8 cycles per scan; **Figure 1Aiii**, **1Biii**), which allows the use of a Fourier analysis to determine the cortical responses [31]. The phase-encoded paradigm only considers activity that is at this signal frequency, excluding low-frequency physiological noise, among other things. The statistical threshold for phase-encoded cortical activity is commonly determined by coherence, which is equal to the amplitude of the blood-oxygenation-dependent (BOLD) signal modulation at the frequency of stimulus presentation (e.g., 6 stimulus cycles per scan), divided by the square root of the power over all other frequencies except the first and second harmonic (e.g., 12 and 18 cycles per scan) [7, 12, 31].

For measuring CFMs of visual space (known as retinotopic or visual field maps), one stimulus set is designed to elicit each voxel's preferred eccentricity typically by presenting

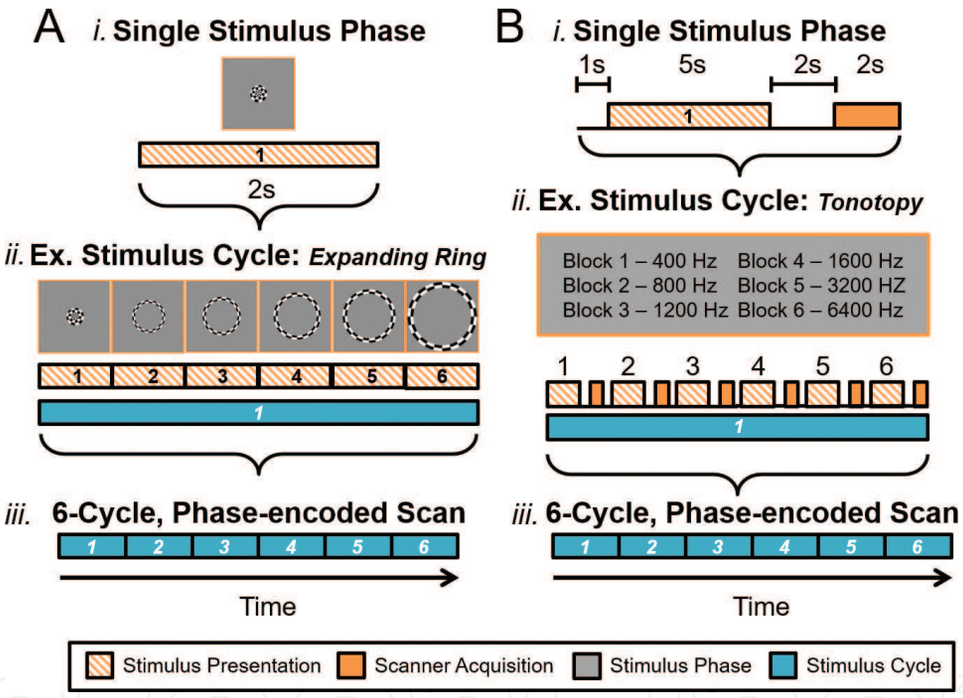

Figure 1. Diagrams of phase-encoded fMRI paradigms for cortical field mapping experiments. **(A)** An example phase-encoded fMRI paradigm for visual field mapping. *(i) Top diagram* shows the components of a single block of one stimulus presentation (striped orange) for one position (i.e., stimulus phase) of an expanding ring stimulus composed of a black and white moving checkerboard pattern. Note that scanner acquisition occurs simultaneously with the stimulus presentation in this case [7, 12]. *(ii) Middle diagram* shows 6 blocks (striped orange) that together compose one stimulus cycle (teal). Each phase of the expanding ring stimulus is displayed above the blocks; one block thus represents one stimulus position in the "phase-encoded" sequence. The term "traveling wave" is also used to describe this type of stimulus presentation, as the stimuli produce a sequential activation of representations across a topographically organized cortical region. *(iii) Lower diagram* displays how 6 cycles (teal)—each repeating the same blocks—compose a full, single scan. **(B)** an example phase-encoded fMRI paradigm for auditory field mapping. *(i) Top diagram* shows the components of a single block of one stimulus presentation (striped orange) followed by an fMRI data acquisition period (solid orange). The sparse-sampling paradigm separates the auditory stimulus presentation from the noise of the scanner acquisition [35]. The timing of the acquisition is set to collect the peak cortical response to the auditory stimulus, in accordance with the approximate hemodynamic delay. *(ii) Middle diagram* similarly shows 6 blocks (striped orange + solid orange) grouped together into one stimulus cycle (teal). Each block, or stimulus phase, in each cycle now represents a specific frequency. An example of this sequence for tonotopic measurements is displayed in Hz. *(iii) Lower diagram* again shows a full, single scan comprising 6 cycles. Note legend in inset.

a high-contrast, flickering checkerboard stimulus shaped like a ring, which expands or contracts in discrete even steps between the central fovea and the periphery to sequentially activate distinct eccentricity representations of visual space (**Figure 1Aii**). The second, orthogonal visual stimulus then activates the preferred polar angle of each fMRI voxel by displaying the same checkerboard pattern now shaped as a wedge spanning a small range of polar angles over all eccentricities. The wedge pattern sequentially activates all polar angles around the central fixation point by rotating clockwise or counterclockwise in discrete steps.

The phase-encoded methods are adapted for auditory field map measurements by combining a phase-encoded stimulus with the sparse-sampling paradigm often used in auditory measurements (**Figure 1B**) [4, 33–36]. Sparse-sampling allows the auditory stimulus presentation to avoid contamination from the noise of the MR scanner during data acquisition by separating the two in time (**Figure 1Bi**) [37–39].

The value of the stimulus (e.g., 5° of visual angle for eccentricity; 400 Hz frequency for tonotopy) that most effectively drives each cortical location is then estimated from the pattern of responses (**Figure 2**). The cortical response at a specific location is said to be "in phase" throughout the scan with the stimulus that most effectively activates it, hence the term "phase-encoded" mapping. The alternative term "traveling wave" arises from the sequential activation of one neighboring cortical location after the other to create a wave-like pattern of activity across the CFM during the stimulus presentation. It is important to note that the phase-encoded methods will not produce a significant BOLD signal in cortex if the stimulus representation in the region is not organized topographically, as there would be no differential activation across the cortical representation [2, 7, 20].

The analysis of phase-encoded cortical field mapping data must be done within individual subjects. Each CFM in sensory cortex can vary dramatically in size and anatomical location across individuals, leading to shifts in cytoarchitectural and topographic boundaries [40–45]. Primary visual cortex, for example, can vary in size by at least a factor of three, independent of brain size [41]. Consequently, when these data are group-averaged across subjects, especially by aligning the data to an average brain through such atlases as Talairach space [46] or Montreal Neurological Institute (MNI) coordinates [47], the measurements are blurred to such an extent that the gradients composing the CFMs are either inaccurate or missing. Relying on whole-brain anatomical co-alignment for cortical averaging will cause different CFMs to be averaged together incorrectly into one measurement, blurring together data from adjacent areas within each subject and making it impossible to differentiate computations in adjacent areas.

2.2. Population receptive field modeling has been developed for measuring visual field maps

A model-based method has been developed for visual field mapping that allows for additional information to be collected about visual field maps (VFMs) by modeling the population receptive field (pRF) of each voxel within a VFM (**Figure 2A**; for complete details, see [48]). Because VFMs are retinotopically organized, the population of RFs in each voxel within a VFM is expected to have similar representations of visual space, allowing for their combined pRF to be estimated as a single, two-dimensional Gaussian. The pRF modeling approach

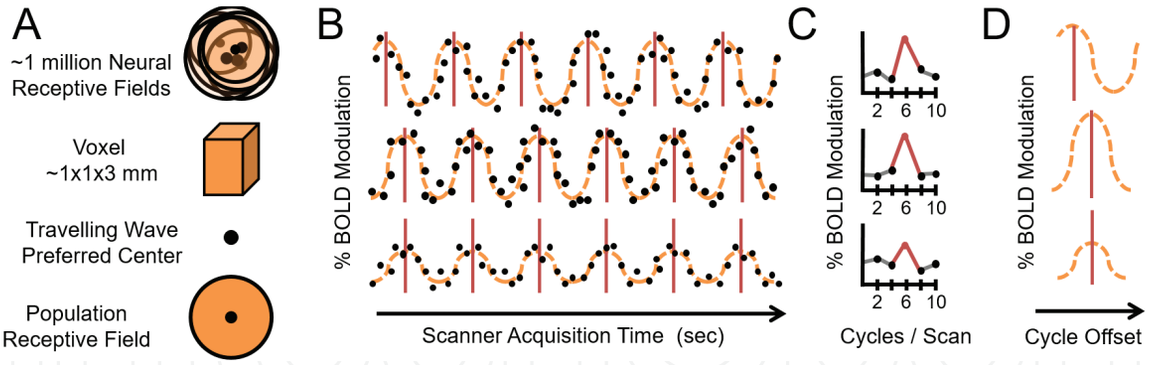

Figure 2. Schematic of measurements of individual voxels in phase-encoded cortical field mapping. **(A)** *Top:* there are on the order of ~1 million neurons within a typical voxel measured with a standardly used 3 T MRI scanner, depending on the size of the voxel [8, 49]. For a voxel within a CFM, the neurons each have similarly tuned receptive fields (orange circles with black outlines) with preferred centers of maximal response (black dots). Note how the overlapping receptive fields concentrate coverage in one region of sensory space (darker orange) corresponding to the average receptive field of the group. *Middle/top:* each typical voxel is on the order of 1 × 1 × 3 mm for cortical field mapping experiments, though voxels are often slightly larger (e.g., 3 × 3 × 3 mm) for other types of experiments [7]. *Middle/bottom:* phase-encoded (i.e., traveling wave) measurements take advantage of the fact that nearby neurons in sensory cortex have similar preferred centers (black dot) in order to estimate an average preferred center for the population of neurons in a given voxel. *Bottom:* Population receptive field (pRF) modeling in visual field mapping takes advantage of the fact that nearby neurons in retinotopic cortex have similar receptive fields in order to estimate not only a preferred center, but also a pRF for the population of neurons in a given voxel [48]. **(B)** Schematic of three example phase-encoded time series with different stimulus responses. Each row represents the activity and analysis of a time series of a single 6-cycle scan of one type of experimental stimuli (e.g., expanding rings) for a single voxel. Black dots indicate simulated raw data points of percent blood-oxygen-level-dependent (BOLD) modulation (i.e., response amplitude). The orange dotted lines represent sinusoidal fits of the simulated data points; each orange line characterizes the average BOLD activation in a different example voxel. The red lines indicate the peak activations per cycle for this imaginary set of voxels. *Top* and *middle rows* represent time series of voxels with the same % BOLD modulation, but different timing of peak responses. This difference in peaks indicates differences in stimulus selectivity (i.e., responses to different "phases" of a stimulus). Note the offset of the red lines between the two rows. For example, the *top row* might represent a voxel with a preferred eccentricity tuning of 3° eccentric to fixation, whereas the *middle row* might have a preferred tuning of 6° eccentric to fixation. *Middle* and *bottom rows* represent time series of voxels with the same timing of peak responses, indicating matching stimulus selectivity; for example, both might have a preferred eccentricity tuning of 6° eccentric to fixation. However, the *bottom row* has much lower % BOLD modulation than the *middle row*. Such a difference in response amplitude can be due to several factors, such as differences in receptive field tuning or local vasculature [8, 11]. **(C)** Schematic of three example Fourier power spectra corresponding to the schematic time series in **(B)**. In the phase-encoded paradigm, only BOLD responses that match the stimulus frequency of 6 cycles per scan (red peak) are considered as data. The responses must also be above a predetermined statistical threshold, typically measured in coherence or percent variance explained [7, 48]. Gray lines denote noise frequencies. **(D)** Schematic of three example averaged stimulus cycles corresponding to the schematic Fourier spectra in **(C)** and to averages of the time series in **(B)**. Each orange dotted line represents the sinusoidal fit for the average, while the peak activation is again marked by the red line. The timing of the peak of each averaged cycle is used to calculate the phase of the preferred stimulus independently for each voxel. Typical pseudocolor overlays on 3-D or flattened brain renderings as shown in **Figures 7** and **10** use color to denote cortical responses to this peak activation (e.g., [4, 12, 33, 34]). Note how the *top* measurement has an earlier peak (red line) that corresponds to an earlier phase of the stimulus (i.e., an earlier presentation time in the cycle) while the *middle* and *bottom* measurements' peaks are shifted to later in time (e.g., [7]). The *bottom* example has a lower % BOLD modulation than the other two schematics, but the same peak activation as the middle example. Adapted from [7].

provides an accurate estimate of not only the preferred center for each voxel's pRF (as with phase-encoded mapping alone), but also its size. In addition, this analysis can be done for any visual stimulus that periodically moves through visual space (e.g., moving bar), rather than just expanding rings and rotating wedges. Research is currently underway to develop a similar pRF model for auditory field maps (AFMs).

3. Fundamental organizing principles of sensory cortex

3.1. What criteria are used to identify a cortical field map?

The term "map" has often been imprecisely applied to topographical gradients or other similar patterns of cortical organization, but the study of cortical sensory processing requires the explicit definition a "cortical field map" according to very precise criteria (**Figures 3** and **4**). First, by definition, each CFM must be composed of at least two orthogonal, non-repeating topographical representations of fundamental sensory dimensions (**Figure 3**) [4, 12, 13, 29, 32]. In the visual system, the retinotopic sensory dimensions arise from the orthogonal aspects of visual space: eccentricity (e.g., center to periphery) and polar angle (e.g., "around the clock") [12, 31]. In the auditory system, the sensory feature space is composed of two aspects of

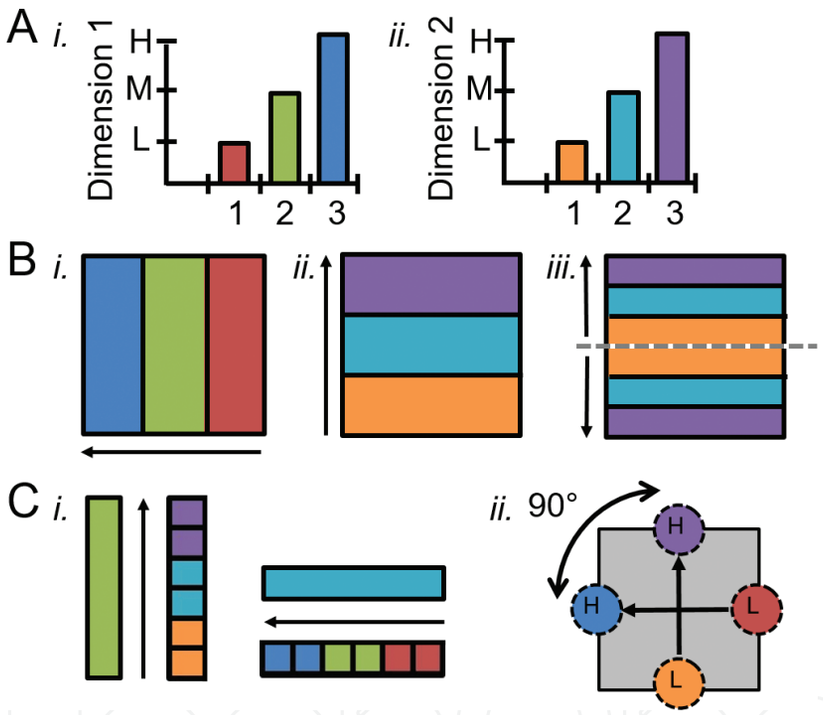

Figure 3. A cortical field map is defined by two orthogonal gradients representing two orthogonal dimensions of sensory space. **(A)** (*i*) Three stimulus values for one sensory dimension (e.g., eccentricity or tonotopy) are depicted in the graph: 1 - low (L, red); 2 - medium (M, green); 3 - high (H, blue). (*ii*) Three stimulus values for a second sensory dimension (e.g., polar angle or periodotopy) are depicted in the second graph: 1 - low (L, orange); 2 - medium (M, aqua); 3 - high (H, purple). **(B)** (*i*) Schematic of a single gradient of dimension 1. Black arrow denotes low-to-high gradient for dimension 1. With only measurements of dimension 1, one cannot determine whether the region within dimension 1 contains one or more CFMs without measuring a second, orthogonal gradient. (*ii*) Schematic of a single gradient of dimension 2 overlapping the dimension 1 gradient in (*i*) to form a single CFM like V1 or hA1. Black arrow denotes low-to-high gradient for dimension 2. Note the orthogonal orientation of the two gradients (*i* vs. *ii*) composing this CFM. (*iii*) Schematic of an alternative gradient organization for dimension 2 overlapping the same dimension 1 gradient in (*i*). Black arrows denote two low-to-high gradients of dimension 2. The dotted gray line denotes the boundary dividing this region into two CFMs. **(C)** (*i*) In a properly defined CFM, measurements along the cortical representation of a single value of dimension 1 (e.g., green) span all values of dimension 2 (e.g., orange to cyan to purple), and vice versa. *(ii)* Schematic of vectors drawn along a single CFM from centers of low-stimulus-value regions of interest (ROIs) to high-stimulus-value ROIs for dimensions 1 (e.g., red to blue) and 2 (e.g., orange to purple). The offset measured between the low-to-high vectors for each dimension should be approximately 90° to be considered orthogonal and thus allow for each voxel/portion of the map to represent a unique combination of dimension 1 and dimension 2 values [4, 7, 10, 12].

http://dx.doi.org/10.5772/intechopen.77964

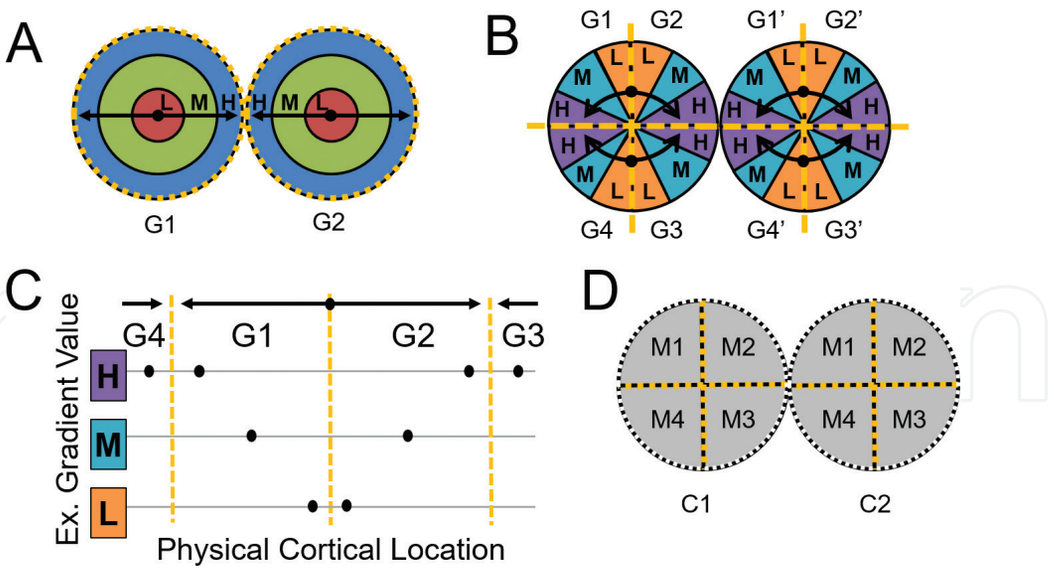

Figure 4. Cortical field map and cloverleaf cluster boundaries are defined along gradient reversals. **(A)** The schematic depicts representations of dimension 1 (e.g., eccentricity or tonotopy) along a flattened cortical surface. Note the repeating patterns of gradient values that denote multiple, repeating representations of low-to-high gradients for the same dimension (e.g., red to green to blue; G1: gradient one; G2: gradient two). Black arrows highlight gradient directions (low, L, to medium, M, to high, H). The gradients for this dimension fall in concentric circles that merge at the outer high (H, blue) representations. Dashed yellow lines mark gradient "reversals" at the edges of the concentric gradients. Note that it is not possible to determine how many CFMs exist within these two gradient sets without additional information from a second representation of an orthogonal dimension. **(B)** The schematic depicts representations of dimension 2 (e.g., polar angle or periodotopy) along the same flattened cortical surface. Again note the multiple, repeating representations of gradient values from low (orange) to medium (cyan) to high (purple) that now run "around the clock" (G3: gradient three; G4: gradient four). Dashed yellow lines mark again mark gradient "reversals," which now are organized like spokes on a wheel. **(C)** The diagram demonstrates how gradient boundaries for one dimension of a CFM are determined. Black dots denote hypothetical measurement points along the cortical surface shown in **(B)**. Arrows and yellow lines are as in **(B)**. Two gradients that span the full range of dimension 2 measurements can be divided into G1 and G2, with the representations of stimulus values increasing from low to high across the cortical surface in one gradient to the boundary where the representations in the next map then reverse back from high to low along the cortical surface in the next gradient. **(D)** Schematic shows the four CFMs defined by these sets of gradients representing the two orthogonal dimensions and arranged in a cloverleaf cluster [4, 7, 9, 10]. Black and yellow dotted lines demark boundaries defined by gradient reversals of dimension 1 and 2 representations, respectively (M1: map one; M2: map two; M3: map three; M4: map four; C1: cluster one; C2: cluster two).

sound: spectral (i.e., tone) and temporal (i.e., period or temporal envelope) information [4, 50]. **Figure 3B** demonstrates the importance of measurements of two orthogonal sensory dimensions for defining CFMs. A region of cortex with a single large gradient for one dimension could denote a single CFM (**Figure 3Bi,ii**) or many CFMs (**Figure 3Bi,iii**). As the number of neighboring gradients increases, the determination of the CFM organization grows increasingly complex. Thus, the number of CFMs in any region cannot be determined without checking for gradient reversals in the representation of the second, orthogonal dimension.

Similarly, two overlapping gradients that are parallel rather than orthogonal will not represent all the points in sensory space uniquely. For example, a region of visual cortex with parallel eccentricity and polar angle gradients would represent a narrow spiral of visual space rather than the entire visual field [7, 20, 51, 52]. Orthogonality can be examined by first estimating the direction of each gradient using a vector drawn from low-to-high stimulus values and then measuring the angle between the vectors for each gradient (**Figure 3Cii**) [4]. In addition, orthogonality can be confirmed by checking that measurements along the cortical

representation of a single value of the first dimension will span all values of the second dimension, and vice versa (**Figure 3Ci**). The orthogonality of each CFM can be determined for individual subjects and can then be compared across the individual subjects.

Second, each of these topographical representations must be organized as an orderly gradient that is generally contiguous (**Figures 3**, **4AB**) [20, 52]. For such a gradient to arise, a large number of voxels must be organized such that they span an entire range of sensory space, in order from one boundary to the other (e.g., from upper to lower vertical meridian for visual polar angle). A topographical gradient is therefore one of the most highly organized features of the cortical surface that we can measure using fMRI; the likelihood of two, orthogonal, overlapping, orderly gradients arising as a spurious pattern from noise is extraordinarily low (for a calculation of the probability of spurious gradients arising from noise, see [11]).

Third, each CFM should represent a substantial portion of sensory space. There may be some differences among CFMs based on the cortical magnification of specific subsets of sensory space, such as the relatively increased foveal representation along the ventral visual cortex, but a large portion of sensory space is still expected to be represented (e.g., [19, 20]). Obtaining a high quality measurement of topographic responses across sensory space is dependent upon choosing a set of phase-encoded stimuli that is appropriate for the sensory domain of interest. The range of values in the stimulus set and the sampling density of those values across feature space both influence the accuracy and precision of the measurement. In addition, the specificity of the representations may undergo some degree of blurring due to such factors as the inherent spatial spread of the fMRI signal, overlapping broad receptive fields, and measurement noise [30, 53–55]. In auditory cortex, in particular, the intensity (or loudness) of the tonotopic stimulus alone can alter the width of the receptive fields of neuron in primary auditory cortex (PAC) and consequently increase the lateral spread of the BOLD signal measured in neuroimaging [56]. Careful consideration should thus be given to the stimulus parameters and how they may affect the cortical responses.

Fourth, the general features of the gradient representations composing the CFMs should be consistent across individuals. It is important to note, however, that even well-accepted CFMs in visual cortex (e.g., V1) can vary dramatically in size and anatomical location [12, 20, 41, 57], as can cytoarchitectural and topographic boundaries in PAC [40, 42–45, 58]. Despite these variations, the general topographical pattern of adjacency among specific CFMs and cloverleaf clusters will be preserved across individuals. The measurement of CFMs provides one of the few *in vivo* ways to localize the distinct borders of a particular cortical region across individuals reliably.

The boundaries of a CFM are determined by carefully delineating the edges of each of the orthogonal gradients measured in a particular cortical region of interest (ROI) within a single hemisphere of an individual subject (**Figures 3** and **4**). Representations of one dimension may be repeated across a region of cortex or may exist in isolation. In isolation, the boundary can be drawn where the gradient responses end, although there will likely be some blurring or spreading of the representation along this edge [12, 20, 31, 48]. Two repeating and adjacent gradients that each span the full range of one dimension (e.g., visual field polar angle) can be divided into two sections at the point at which the gradients reverse (**Figures 3B**, **4**). At the gradient reversal, the representations of stimulus values increase

http://dx.doi.org/10.5772/intechopen.77964

from low to high (or vice versa) across the cortical surface in one section to the boundary where the representations in the next CFM then reverse back from high to low (or vice versa) along the cortical surface in the next section (**Figure 4C**).

3.2. How are cortical field maps distinguished from sensory gradients or cortical areas?

A pervasive mistake in cortical field mapping has been the attempt to define a CFM using only a single cortical gradient (for reviews, see [2, 7, 8]). As described above, it is vital to understand that the representation of one dimension of sensory space – one topographical gradient along cortex – is not sufficient to define a CFM (**Figures 3**, **4**). A lone gradient simply reveals that this particular feature of sensory space is represented in that region of cortex.

In addition, we describe measurements of "cortical field maps" rather than use the phrase "cortical areas," as the definition of CFMs is specifically coupled to the topographical measurement, while cortical area definitions are based on a different and potentially conflicting set of criteria. Cortical areas have most extensively been identified in visual and auditory cortex using various combinations of the following measurements: 1) cytoarchitecture, 2) patterns of connectivity, 3) topography of sensory representations, and 4) functional responses [6, 7, 12, 20]. Because these separate types of measurements can at times produce conflicting results, the definition of cortical areas has led to many controversies in the naming of sensory areas. Observations of one or two cortical area criteria have often been used to propose the presence of a distinct cortical area; such definitions may then view the topography – the defining feature of CFMs – as secondary. Multiple CFMs may be present within what has been otherwise defined as a single cortical area. For example, cytoarchitecture was used to define Brodmann areas 18 and 19, which compose much of occipital visual cortex beyond primary visual cortex (V1). However, this same region of visual cortex is tiled with numerous VFMs (for additional discussion, see [7, 12]). Because of the significant complexity and confusion that such conflicting definitions can produce, our understanding of how to divide up cortex into distinct regions is still evolving and our naming schemes may vary based on the level of processing we are considering (e.g., first-order vision motion computations vs. the entire visual motion processing pathway). For current investigations of human visual and auditory cortex, sensory system researchers primarily rely on the topographical measurement of CFMs, which is the most well-established the measurement of cortical areas in the *in vivo* human brain at this time [7, 12].

3.3. Cloverleaf clusters: macrostructural organization of cortical field maps

Groups of adjacent CFMs have now been shown by multiple laboratories to be organized within visual and auditory cortex into a macrostructural pattern called the cloverleaf cluster. These clusters of CFMs have been described as a cloverleaf due to the organization of the individual CFMs within the cluster appearing like the leaves of a clover plant (**Figure 4D**). Brewer and associates first described cloverleaf clusters in human visual cortex [2, 7, 12, 20]; subsequent measurements demonstrated the presence of these clusters in other parts of human visual cortex [10, 11], in macaque visual cortex [9], and in human auditory cortex [4].

Figure 4 demonstrates how CFMs are arranged in a spatial pattern of clusters at a scale of several centimeters. Cloverleaf clusters are composed of groups of adjacent CFMs; one dimension of sensory topography is represented in concentric, circular bands from center to periphery of the cluster (e.g., vision: eccentricity; audition: tonotopy; **Figure 4A**), and the second, orthogonal dimension divides this confluent representation into multiple CFMs with radial bands spanning the cluster center to periphery (e.g., vision: polar angle; audition: periodotopy; **Figure 4B**). This type of macrostructural organization is now referred to as being radially orthogonal [7]. While the namesake clover plant is most commonly seen with a four-leaf organization, cloverleaf clusters may contain any number of CFMs. However, only an even number of CFMs will produce a smooth progression of representations around the cluster from the border of one CFM to the next. Measurements to date have shown that these clusters have consistent locations relative to one another, but that the maps within each cluster may be oriented somewhat differently, as if, in each individual's brain, the clusters themselves each may be positioned at a slightly different rotation about the cluster's central representation. Such inter-subject variability in cloverleaf cluster positions is consistent with our understanding of the variability in molecular gradient expression underlying the development of topographical gradients in cortex [26, 59–62]. Careful analysis across individual subjects can identify common CFMs by analyzing the pattern of CFMs and cloverleaf clusters across sensory cortex. This variability in cluster rotation and as well anatomical location again highlights the need for individual-subject data analysis.

The cloverleaf cluster organization of the CFMs may be important not only for the definition of CFMs, but may also play a role in coordinating neural computations. Neurons within each cluster are thought to share common computational resources. For example, CFMs within a cluster might have common mechanisms to coordinate neural timing or short-term information storage [2]. Similarly, it is likely that functional specializations for perception are organized by cloverleaf clusters rather than by single CFMs [20, 63]. VFMs within a cluster, for example, have very similar total surface areas, and each cluster's total surface area is reliable across subjects [11]. Each cloverleaf cluster can be functionally differentiated by its pattern of coherence measurements (i.e., BOLD response), cortical magnification, and pRF sizes. These distinctions indicate that VFMs within individual cloverleaf clusters are not only anatomically but also functionally related [7, 9, 17]. The cluster organization is not necessarily thought to be driving the common functions, but rather reflects how multiple stages in a sensory processing pathway might arise during development across individuals and during evolution across species.

4. The visual system

4.1. Overview

The visual field spatial arrangement is a fundamental physical property of a visual image [2]. While an image may still be identifiable despite alterations of such properties as its color, motion, contrast, or rotation, scrambling its spatial arrangement typically destroys our ability to identify or reconstruct the original image. This visual field spatial arrangement is encoded by the circuitry of the retina and then preserved and repeated through visual cortex

to produce a unifying matrix of visuospatial organization throughout the visual processing hierarchy, despite the diverse computations being performed across regions (e.g., [7, 12, 64]). As cortex interprets different aspects of the visual image—such as its motion or orientation—the cortical circuitry is organized using receptive fields organized within VFMs to preserve the critical spatial image information.

Neurons in lower-level VFMs perform computations on low-level visual features within a specific retinal location; these computations grow increasingly complex as the stimulus features are processed along the cortical hierarchy. Even though they may contain neurons primarily with large receptive fields, higher-order visual regions may still preserve the visuospatial organization of the image on the retina by retaining sufficient dispersion of receptive field centers through slight differences in the preferred tuning of neuronal responses to visual space [65]. Thus the occurrence of retinotopic organization in higher-order areas can still provide the position and stimulus size invariances typically attributed to high-order object- and face-responsive visual regions [7, 11, 48, 66, 67]. Current research is demonstrating that the majority of higher-order visual areas are organized according to visual space, maintaining retinotopically organized, dispersed receptive field centers despite increasingly large receptive field sizes [7, 11, 19, 65, 68–73].

Whether the spatial organization in visual cortex remains truly retinotopic or changes to a broader spatiotopic organization – one based on external space rather than retinal space – is still under investigation and cannot be determined with typical visual field mapping methods [69, 70, 74, 75]. In any case, this extensive preservation of visuospatial organization produces a common frame of reference for passing information up or down the visual hierarchy. Such visual-location-based "channels" could explain how higher-order areas subserving visual-attention can simultaneously influence many lower-level visual areas in spatially specific patterns [74, 76–80]. Another option may be that retinotopic organization is preserved across the cortical hierarchy even without a critical role for visual location information in the computations of a higher-order cortical region merely because changing the neuronal arrangement after it is established at the level of the retina and early visual cortex may be too costly or disruptive during development.

4.2. Low-level VFMs are arranged within a cloverleaf cluster on the medial occipital surface

Human visual cortex includes the entire occipital lobe and extends significantly into the parietal and temporal lobes (**Figure 5**), composing about 20% of cortex [12]. The medial wall of occipital cortex in each hemifield contains four hemifield representations of visual space known as V1, V2, V3, and hV4 (**Figures 6**, **7**; for detailed reviews, see [7, 12]). V1 consistently occupies the calcarine sulcus, bounded on either side by the split-hemifield representations of V2 and V3 on the lingual gyrus and cuneus. Human V4 (designated hV4 because of the unclear homology to macaque V4) is positioned as a complete hemifield on the ventral occipital surface adjacent to ventral V3 along the posterior fusiform gyrus [20, 82]. These four VFMs compose the medial aspect of the occipital pole cluster (m-OP cluster), which supports low-level visual computations [2, 7, 20].

Because it receives direct inputs from the retinogeniculate pathway, V1 is considered to be primary visual cortex, and it is the first place in retina-to-cortex pathway where information

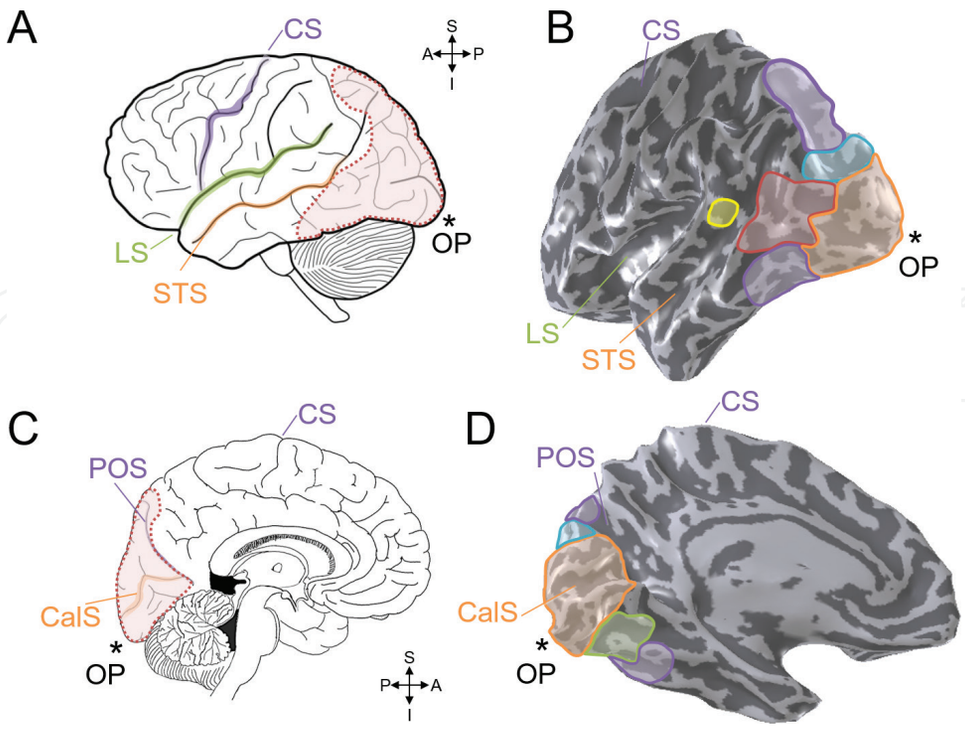

Figure 5. Visual cortex in the human brain. **(A)** Diagram of the lateral view of the human left cerebral hemisphere. Black lines denote major sulci. The general location of visual cortex is marked in red within the red dotted line [7, 12]. CS: Central sulcus (purple); LS: lateral sulcus, also known as the lateral or Sylvian fissure (green); STS: superior temporal sulcus (orange); OP*: occipital pole. Inset legend shows approximate anatomical directions for the views in **(A, B)**. S: superior; I: inferior; A: anterior; P: posterior. **(B)** 3-D rendering of the lateral view of an individual left hemisphere cortical surface. Light gray indicates gyri; dark gray indicates sulci. The locations of several VFM cloverleaf clusters as well as regions currently under investigation are shown by the colored ROIs: orange, OP cluster (occipital pole cluster, lateral subdivision including LO-1, LO-2, LOC) [2, 7, 81]; cyan, V3A/B cluster [2, 13]; red, hMT+ cluster (human medial temporal complex, V5) [2, 4, 9, 10, 12]; yellow, pSTS cluster (posterior superior temporal sulcus) [11]; purple, regions along the dorsal cortex (intraparietal sulcus) and ventral cortex (fusiform and parahippocampal gyri) currently under investigation (for reviews, see [4, 12]). **(C)** Diagram of the medial view of the human left cerebral hemisphere. Inset legend shows approximate anatomical directions for the views in **(C, D)**. POS: Parietal-occipital sulcus (purple); CalS: calcarine sulcus (orange). Other details are as in **(a)**. **(D)** 3-D rendering of the medial view of the left hemisphere cortical surface from the same individual. The locations of several VFM cloverleaf clusters as well as regions currently under investigation are again shown by the colored ROIs (n.b., clusters that span medial and lateral cortex match in color): orange, OP cluster (medial subdivision including V1, V2, V3, hV4) [2, 7]; cyan, V3A/B cluster; green, VO cluster (ventral occipital) [2, 20]; purple, dorsal and ventral regions currently under investigation. Other details are as in **(B)**.

from the two eyes is combined to form binocular cells. In addition, V1 is an important site of basic calculations such as orientation, color, and motion. Each computation is performed across the entire visual field, yet V1 appears at the level of fMRI measurements consist of a single, contiguous representation of visual space. In essence, V1 is composed of several VFMs overlaid on one another, each of which performs a single computation (i.e., separated maps for color, orientation, and motion). In this arrangement, a very intricate mosaic of neurons subserving these computations allows for each computation to be performed over each portion of the visual field. These mosaics, including pinwheel orientation columns, blobs/interblobs, and ocular dominance columns, are still being extensively investigated (e.g., [83–85]). These computations divide up into more specialized processing of the visual image after V1, with V2 and hV4 supporting low-level color and form processing, respectively, and V3 playing a role in low-level motion computations [12, 20, 51].

http://dx.doi.org/10.5772/intechopen.77964

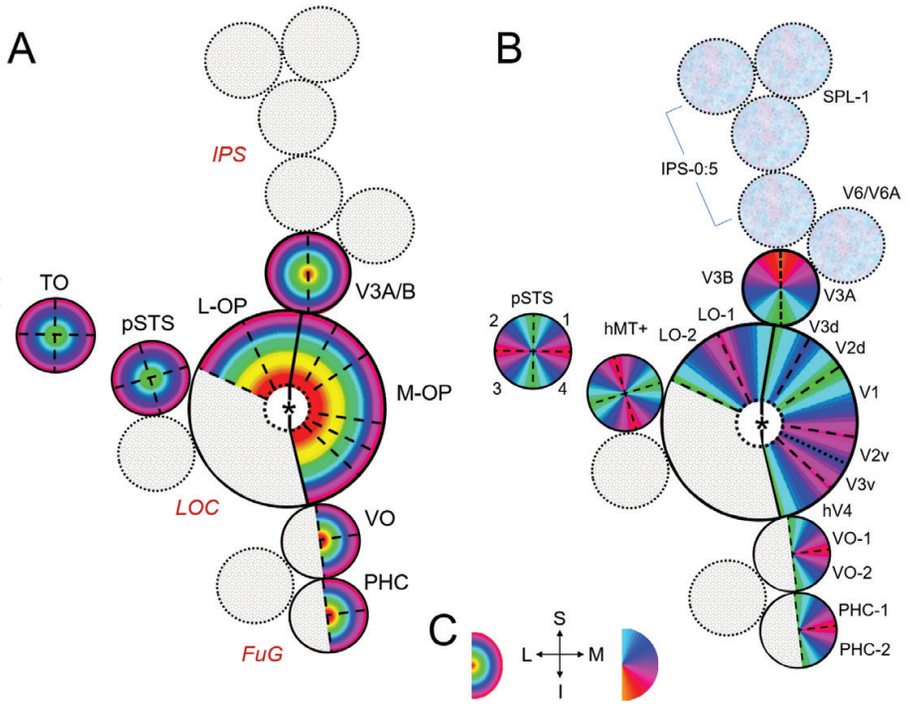

Figure 6. Schematic of human visual field map clusters. Schematics of eccentricity and polar angle representations within VFM clusters as would be viewed on a flattened left hemisphere. Color overlays represent the position in visual space that produces the strongest response at that cortical location. "*" marks occipital pole. Gray regions denote areas in which cloverleaf clusters are currently being investigated. **(A)** Diagram of eccentricity representations. Black labels denote published clusters: M-OP, medial aspect of occipital pole cluster; L-OP, lateral aspect of occipital pole cluster (partially defined); V3A/B, visual areas 3A and 3B cluster; TO, temporal occipital cluster; pSTS, posterior superior temporal sulcus cluster; VO cluster, ventral occipital cluster (partially defined); PHC cluster, parahippocampal cluster (partially defined). Red italicized labels denote anatomical regions currently under investigation: IPS, intraparietal sulcus; LOC, lateral occipital cortex; FuG, fusiform gyrus. **(B)** Diagram of polar angle representations. Black labels denote VFM names. Blue-magenta textured circles along IPS denote regions where polar angle representations have been measured, but not consistent eccentricity gradients. **(C)** *Right:* Color legend for eccentricity representations. *Middle:* Legend inset denotes approximate anatomical locations for the schematic. S: Superior; I: inferior; L: lateral; M: medial. *Left*: Color legend for polar angle representations.

V1, V2, V3, and hV4 each contain a foveal representation positioned at the occipital pole, with progressively more peripheral representations extending into more anteromedial cortex, forming complete eccentricity gradients (**Figure 7Ai,Bi,Ci**; e.g., [12, 29, 30, 32]). The region where the individual foveal representations meet at the occipital pole is commonly termed the "foveal confluence" [86]. Although fMRI measurements of eccentricity gradients depict these foveal representations as merging into one combined foveal region, careful fMRI measurements of polar angle gradients have demonstrated that distinct boundaries exist between even the most central foveal representations of V1, V2, V3, and hV4 [20, 86, 87].

The boundaries between each map are delineated by reversals in the polar angle gradients along the medial surface (**Figure 7 Aii**, **Bii**, **Cii**; e.g., [12, 29, 30, 32]). V1 has a contiguous polar angle gradient representing a full hemifield, while V2 and V3 have split-hemifield representations (i.e., quarterfields), which are named by their positions ventral or dorsal to V1: V2d, V2v, V3d, V3v. Because of their relatively consistent anatomical locations and unique concentric polar angle gradients, these three VFMs are typically the first landmarks identified in visual field mapping analyses [31, 32]. However, as noted above, the surface areas of these

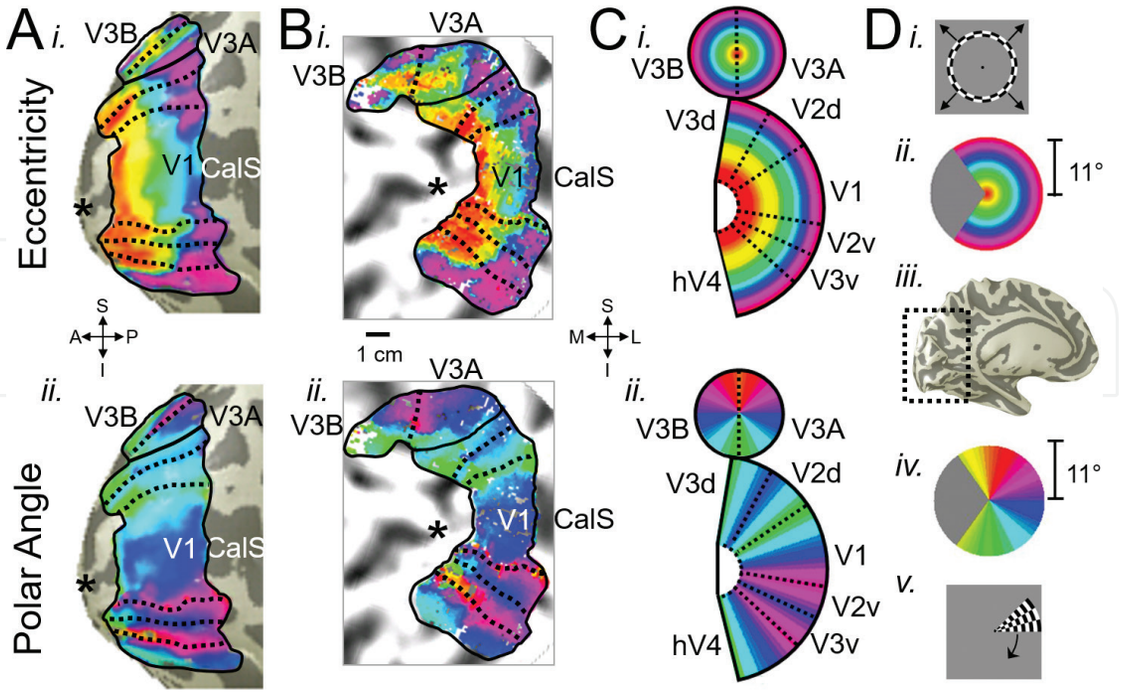

Figure 7. Example visual field map cloverleaf cluster data in human cortex. The pseudocolor data overlays on inflated 3-D **(A)** and flattened **(B)** representations of a single left hemisphere of one subject and the colors in the schematic **(C)** represent the location in visual space that creates the strongest response at that cortical position (see color legends in **(D)**). Solid black lines mark VFM boundaries at peripheral eccentricity reversals, which separate cloverleaf clusters from each other. Dotted black lines denote VFM boundaries along polar angle reversals, which separate individual VFMs within cloverleaf clusters. Light gray on the inflated/flattened cortex images indicates gyri; dark gray indicates sulci. **(A)** (*i*) Eccentricity gradient data are shown for the medial OP cluster and the V3A/B cluster. (*ii*) Polar angle gradients within the same VFM clusters are displayed. Inset legend denotes the anatomical orientation for the inflated brain images; A: anterior; P: posterior; S: superior; I: inferior. **(B)** (*i*) A view of the same eccentricity gradients is now shown on a flattened view of the cortical sheet. (*ii*) A view of the polar angle gradients within the same VFM clusters is displayed. Inset legend denotes the anatomical orientation for the flattened brain images. M: Medial; L: lateral; S: superior; I: inferior. Scale bar signifies 1 cm along the flattened cortical surface. **(C)** (*i*) Schematic of the eccentricity gradients of these VFM clusters; (*ii*) schematic of the polar angle aspect of these VFM clusters. VFMs within these clusters are labeled here and correspond to the VFMs displayed in **(A, B)**. **(D)** (*i*) One phase of the expanding ring stimulus used to measure eccentricity. (*ii*) color legend for eccentricity representations; (*iii*) inflated 3-D brain rendering, with dotted lines and arrow indicating the cropped view shown in **(C)**; (*iv*) color legend for polar angle representations; and (*v*) one phase of the rotating wedge stimulus used to measure polar angle. All data for **(A–D)** are from the left hemisphere of one subject collected using phase-encoded fMRI paradigm with moving-bar visual stimuli spanning 11° of visual angle. Coherence ≥0.25. Adapted from [11].

three VFMs fluctuate significantly among individuals independent of overall brain size [41]. While V1 is always located along the fundus of the calcarine sulcus in normal individuals, an increase in V1 size will consequently shift the specific positions of V2 and V3 along the neighboring gyri and sulci. VFMs beyond V3, such as the contiguous hV4 hemifield, continue to shift variably along the cortical surface in accordance with variable individual VFM sizes.

4.3. VFMs compose several cloverleaf clusters along the ventral stream

Several more VFMs representing extensive, contiguous hemifields of visual space are positioned along the fusiform gyrus anterior to hV4 (**Figures 5 BD**, **6**, **7**). These VFMs are named by their anatomical location and number within a cluster: VO-1 and VO-2, for ventral-occipital cortex, and PHC-1 and PHC-2, for parahippocampal cortex. VO-1

and VO-2 partially compose the VO cluster, share a distinct foveal representation, and subserve mid-level color and form processing [20]. Similarly, PHC-1 and PHC-2 partially compose the PHC cluster, share another discrete foveal representation, and display varying degrees of scene selectivity [19]. The eccentricity gradients reverse between clusters along the ventral surface, while the polar angle gradient reversals again divide up the clusters into individual hemifield VFMs.

In contrast to the measurements in posterior medial and VFMs, it has been much more difficult to measure retinotopic organization within the lateral occipital cortex, a region encompassing the object-responsive lateral occipital complex (LOC; **Figures 5B**, **6**). The LOC was originally thought to lack retinotopic organization or have only an "eccentricity bias" [88–90]. Recent studies along the dorsal aspect of the LOC, however, have described two VFMs, called LO-1 and LO-2 for "lateral occipital" (**Figure 6**). LO-1 is positioned just anterior to the lateral aspect of V3d, reversing from the upper vertical meridian representation at the boundary into its representation of a full hemifield of visual space with the hemifield of LO-2 at its inferior edge [81, 91]. The foveal representations of these two VFMs join with the confluent foveal representations of V1, V2, V3, and hV4 on the occipital pole to form part of the lateral aspect of the occipital pole cluster (l-OP cluster). In addition, regions just inferior to LO-2 have been shown to be responsive to lateralized visual stimuli, but have not yet been divided into specific VFMs [92–95]. Emerging data suggest that lateral occipital cortex inferior to LO-2 will also consist of multiple VFMs, which would complete the l-OP cluster subserving mid-to-high level object recognition. As noted above, the responses to object stimuli in this region could remain both invariant to stimulus size and position over a wide field of view while retaining visuospatial information [67].

4.4. VFMs also compose several cloverleaf clusters along the dorsal stream

4.4.1. Lateral occipital-temporal cortex

Just anterior to LOC along the bank of the inferior temporal sulcus, motion-selective cortex comprises a distinct cloverleaf cluster, alternatively known as the TO (temporal-occipital) or MT (medial-temporal) cluster (**Figures 5B**, **6**) [2, 10, 96, 97]. This cloverleaf cluster consists of the four VFMs of the hMT+ (human MT complex) thought to be involved in successive stages of visual motion processing [9, 10, 96, 98, 99]. The dorsal two hemifield VFMs are positioned just anterior to the LO maps, merging with that cluster at an eccentricity gradient reversal. These VFMs have been alternatively termed TO-1 and TO-2 or MT and MST, respectively, based on the likely homology to the VFMs of the MT cluster in macaque monkey [9, 10, 97]. These two VFMs share a distinct foveal representation with two VFM along more ventral lateral occipital cortex that are likely homologous to macaque FST and V4 t.

Anterior, but not adjacent, to the TO cluster, is a recently discovered additional cloverleaf cluster on the posterior superior temporal sulcus (pSTS): the pSTS cluster (**Figures 5B**, **6**) [11]. The pSTS clusters consists of four VFMs labeled pSTS-1, pSTS-2, pSTS-3, pSTS-4 and is located in a region implicated in high-order visual processing dealing with complex aspects of face and motion processing [100, 101]. In addition, this cortex has been associated with high-order multisensory processing, including the integration of auditory and visual information about objects [102, 103]. Thus, these CFMs may have multimodal tuning.

4.4.2. VFMs, cloverleaf clusters, and polar angle gradients in dorsal parietal and frontal cortex

Beyond the medial half of the dorsal boundary of V3d, a series of hemifield VFMs run from the transverse occipital sulcus (TOS) up along the intraparietal sulcus (IPS) (**Figures 5B**, **6**; e.g., [12, 76]). The first VFMs here bordering V3d are V3A and V3B, which share a discrete foveal representation within the TOS (**Figure 7**) [11, 13, 104, 105]. Measurements of V3A suggest that it has some similarities to macaque V3A and V3d, and it is thought to play a role in motion processing; the computations subserved by V3B are not yet resolved, but the basic parameters of its computations match that of V3A [11, 13, 104, 106, 107].

Moving anteriorly along the IPS from V3A and V3B, measurements find that visuospatial responses here are activated by attentionally demanding, phase-encoded stimuli, consistent with the description of this parietal region as subserving spatial attention [70, 74, 77–79, 106, 107]. The first VFM along the IPS is IPS-0 (formerly called V7), which has a foveal representation distinct from the one shared by V3A and V3B and represents a full hemifield of contralateral visual space [77, 107]. A series of polar angle representations then runs from IPS-0 along the medial wall of the IPS (**Figure 6B**). These representations have primarily been described as reversing smoothly through a strip of several hemifield representations from IPS-0 to IPS-5, with another polar angle representation termed SPL-1 (superior parietal lobule) just medial to these maps [70–72, 74, 76, 77, 79, 108]. Also along the medial wall of the parietal cortex and just anterior to V3d in the parieto-occipital sulcus are two additional polar angle gradients involved in particular types of motion processing, such as self-motion and visuomotor integration: V6 and V6A [109, 110]. V6 and V6A both contain relatively coarse polar angle representations of the contralateral hemifield and potentially eccentricity representations of the far periphery. It is important to note that, except for V6, these parietal representations are all descriptions of polar angle gradients rather than complete VFMs (**Figure 3**). Thus the full extent of VFMs and cloverleaf clusters along the IPS remains to be determined [7].

Several polar angle representations of the contralateral hemifield have also been measured in frontal cortex by a few studies using a variety of stimuli including phase-encoded paradigms, memory-guided saccade tasks, and visual spatial attention tasks (**Figure 6B**) [69, 70, 73, 76, 78, 79]. These topographic representations are positioned in precentral cortex (pre-CC), dorsolateral prefrontal cortex (DLPFC), the frontal eye fields (FEF), and the supplementary eye fields (SEF), cortical regions involved in the complex visual processing of spatial attention and eye movement control. Like the polar angle measurements along the IPS, these frontal regions also lack measurements of orthogonal eccentricity representations. As research progresses, we expect overlapping eccentricity gradients will be found, forming VFMs likely organized into cloverleaf clusters.

5. The auditory system

5.1. Overview

The auditory system encodes the complex sound waves we encounter in our daily environments as the intensity of their individual component frequencies, analogous to a Fourier analysis (**Figure 8A**). Higher frequency variations are transduced near the opening of the

cochlea of the inner ear, with decreasing frequencies transduced further down the membrane. This topographic gradient of frequencies, or tones, from low to high is referred to as tonotopy (or, less commonly, cochleotopy – a map of the cochlea). Spectral sound representation in the form of tonotopic gradients is thus one aspect of the fundamental auditory reference frame. This basic auditory information and tonotopic organization is preserved through multiple subcortical areas and at least through low-level auditory cortex (for reviews, see [8, 111–113]).

The second, orthogonal aspect of the fundamental auditory reference frame is temporal sound information, termed periodicity (**Figure 8B**) [4, 114, 115]. Periodicity information is thought to be coded in the auditory nerve through neural activity time-locked to the periodicity of the amplitude modulation (i.e., the length of time from peak-to-peak of the temporal envelope) [114, 116]. The temporally varying aspects of sound are expected to be encoded by neurons tuned to sounds of certain durations as well as neurons selective for the onset and offset of sounds Periodotopy thus refers to the topographic organization of neurons that respond differentially to sounds of different temporal envelope modulation rates.

Auditory processing in human and non-human primate cortex resides bilaterally within the temporal hemispheres near the lateral sulcus (**Figure 9A**) [8, 42, 117–121]. In the model system of macaque monkey, the first stage of cortical processing lies along the superior temporal gyrus (STG) and consists of three primary auditory areas: A1, R, and RT [122]. In contrast to visual cortex in which V1 is a single area defined as primary visual cortex, primary auditory cortex is

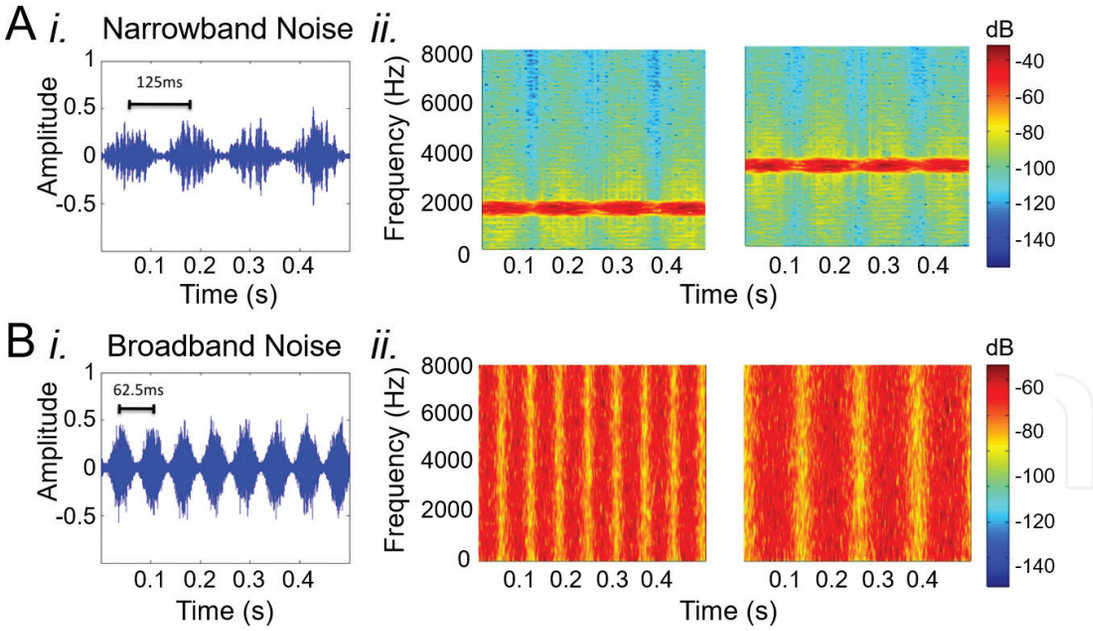

Figure 8. Example auditory field mapping stimuli. **(A)** Examples of a narrowband noise stimulus set (*i*) sound amplitude (arbitrary units) for this stimulus set as a function of time in seconds. (*ii*) Sound spectrograms for two narrowband noise stimuli with center frequencies (CF) of 1600 Hz (*left*) and 3200 Hz (*right*). Higher amplitudes in decibels (dB) are represented as "warmer" colors across frequencies (vertical axis, dB legend on right) and time in seconds (horizontal axis). **(B)** Examples of a broadband noise stimulus set (*i*) sound amplitude (arbitrary units) for this stimulus set as a function of time in seconds. (*ii*) sound spectrograms for two broadband noise stimuli with amplitude modulation (AM) rates of 8 Hz (*left*) and 16 Hz (*right*). Higher amplitudes are again represented as "warmer" colors across frequencies (vertical axis, dB legend on right) and time in seconds (horizontal axis). Narrowband noise stimuli hold periodicity constant and vary frequency, while broadband noise stimuli maintain constant frequency information and vary periodicity.

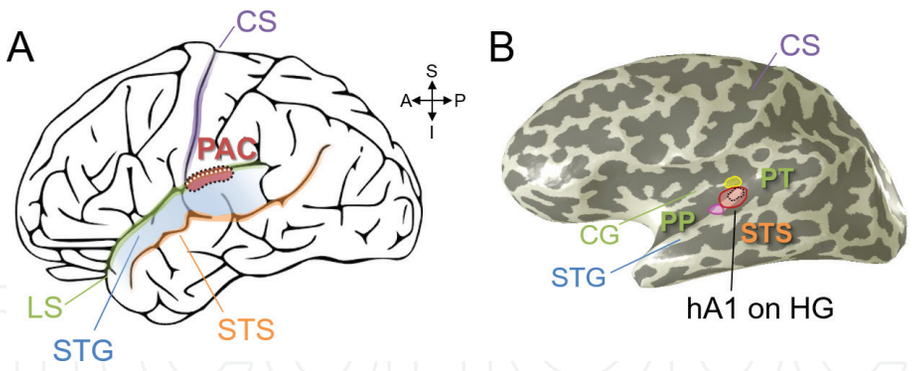

Figure 9. Early auditory cortex in the human brain. **(A)** Diagram of the lateral view of the human left cerebral hemisphere. Black lines mark major sulci. The approximate location of primary auditory cortex (PAC) is denoted by the red overlay within the black dotted line. The white dotted line within the red area shows the spread of PAC into the lateral sulcus (LS) along Heschl's gyrus (HG) that is not visible in this view. Inset legend shows anatomical directions for both brain images. S: Superior; I: inferior; A: anterior; P: posterior. PAC: primary auditory cortex (red); CS: Central sulcus (purple); LS: lateral sulcus, also known as the lateral or Sylvian fissure (green); STG: superior temporal gyrus (blue); STS: superior temporal sulcus (orange). **(B)** Inflated 3-D rendering of an individual left hemisphere cortical surface. Light gray indicates gyri; dark gray indicates sulci. The specific location of the hA1 auditory field map for this subject is marked with the black dotted lines. hA1 lies at the tip of HG. Note that HG is a single gyrus in this subject. CG: Circular gyrus (green); PP: planum polare (green); PT: planum temporale (green). Green labels are sections within LS. The three colored ROIs on HG denote the locations of the cloverleaf clusters comprising the core and belt AFMs: Yellow, hCM/hCL cluster; red, HG cluster including hA1, hR, hRM, hMM, hML, hAL; magenta, hRTM/hRT/hRTL cluster [4, 8]. Additional cloverleaf clusters are under investigation in the surrounding regions of auditory cortex along LS.

considered to be a core of these three AFMs, as all three contain the dense thalamic inputs from the thalamus, the expanded layer IV, and the high expression of cytochrome oxidase, acetylcholinesterase, and parvalbumin characteristic of primary sensory cortices [117, 118, 121, 123–128]. Secondary levels of cortical processing are then mediated by a set of eight belt regions, situated with four areas along both the lateral (CL, ML, AL, RTL) and medial (CM, RM, MM, RTM) sides of the core [129–131]. On the lateral side of the belt, an additional two regions compose the parabelt, which serves as a tertiary level of auditory processing that distributes information to neighboring auditory regions as well as multimodal areas across cortex [123, 132].

Due in part to methodological limitations, many studies of human audition over the past few decades have focused on psychoacoustics research of audition at the behavioral level or on neuroimaging investigations of speech production and comprehension in high-order cortex. In contrast, research about the structure and function of lower-level auditory processing in human cortex has been comparatively limited. An understanding of how lower-level auditory cortex is organized is crucial, however, for expanding our understanding of both the cortical pathways supporting basic auditory behavior and the auditory inputs available to speech processing networks.

Recent research has revealed that the cortical organization underlying lower-level human auditory processing resembles that of macaque core, belt, and parabelt structure, but with a rotation of these regions from the STG to Heschl's gyrus (HG), an anatomical structure within the lateral sulcus unique to humans (**Figure 9**) [4, 43, 58, 121]. The human auditory system also has similarities to the human visual system at several levels, from the fundamental organization of processing lower-level auditory information within AFMs and cloverleaf clusters

[4, 8] to the dual-stream model for higher-level speech processing in which ventral pathways support comprehension and dorsal pathways subserve sensorimotor integration [133]. AFMs, like VFMs, comprise two orthogonal representations of dimensions of sensory feature space: tonotopy (maps of tones, the spectral content of sounds) and periodotopy (maps of periods, the temporal content of sounds). Furthermore, these AFMs are organized into several cloverleaf clusters; the discovery of this cross-modal presence of cloverleaf clusters demonstrates that such cluster organization is a fundamental aspect of sensory cortex (**Figures 9**-**11**) [4, 134].

5.2. AFMs compose three cloverleaf clusters overlapping Heschl's gyrus

The history of auditory field mapping was complicated by the long delay between our ability to measure tonotopic gradients in human cortex and the discovery of human and non-human primate orthogonal periodotopic representations. Basing their investigations on only tonotopic responses, neuroimaging researchers futilely attempted to reach a consensus about the organization of human auditory cortex. As expected from schematics in **Figure 3**, the measurement of only one topographical representation led to a number of variable, conflicting, and ultimately unusable interpretations of the organization of human PAC and surrounding regions (for detailed discussions, see [8, 134]).

The relatively recent discoveries of periodotopic gradients in the macaque monkey midbrain brain and human auditory cortex have now allowed for an accurate definition of the first auditory field maps [4, 115]. This finding is supported by evidence from human psychoacoustic studies, which show that separable filter banks exist not only for frequency spectra, but also temporal information, signifying the presence of neurons with receptive fields tuned to ranges of frequencies and periods [50, 135–137]. Additionally, gradients representing temporal acoustic information have been measured in other animal models, including domestic cat PAC and chinchilla inferior colliculus [82, 138].

Eleven AFMs have been defined in human auditory cortex to date and show clear homologies to the eleven core and belt subfields of auditory cortex identified in human cytoarchitectural studies and in non-human primate cytoarchitectural, connectivity, and tonotopic measurements (**Figures 10**, **11**) [4, 8, 42, 118, 119, 122, 123, 126, 139–141]. The naming of the human AFMs follows that of the suspected homology to macaque, but appends an "h" to indicate human [4].

Three separate sets of concentrically organized tonotopic gradients overlap HG, running from STG to the circular sulcus (CiS; **Figure 10A**, **11C**). The first complete auditory cloverleaf cluster measured in humans – the HG Cluster – is centered on the primary, circular tonotopic gradient on Heschl's Gyrus (HG; **Figures 9**-**11**) [8]. The low-tone representation in this cluster is positioned centrally and expands in iso-tone bands out to high-tone representations. A reversal in the anteromedial high-tone region of the HG cluster divides the HG cluster from the CM/CL cluster. Abutting the HG cluster where HG meets STG, there exist another tonotopic reversal into the RT cluster. More research is required to determine the full extent of the CM/CL and RT clusters.

Periodotopic gradient reversals along HG divide the tonotopic representation of the central HG cluster into two AFMs each of core, medial belt, and lateral belt: hA1, hR, hMM, hRM, hML, and hAL (**Figures 10B**, **11D**). HA1 lies within this cluster at the tip of HG and is the largest of the core and belt AFMs. It is thought to subserve the most basic of cortical auditory computations, and this is reflected in its detailed tonotopic and periodotopic gradients [123]. The anterior/medial aspect of hA1 is tuned to high tones, and the posterior/lateral aspect is tuned to low tones. Just past the tip of HG and the high-tone reversal in the circular sulcus (CiS), a high-periodicity gradient reversal divides the tonotopic representation of the CM/CL cluster into hCM, and hCL, two regions that have been implicated in early language and speech processing as well as audiovisual integration [142]. Similarly, at the base of HG, a set of periodotopic gradients divides the partial third cloverleaf cluster into hRT, hRTM, and hRTL. These AFMs along STG in macaque have been shown to be involved in lower-level processing of stimuli like temporally modulated environmental sounds [129, 130]. Now that these AFMs and cloverleaf clusters can be reliably identified in individual subjects, researchers can

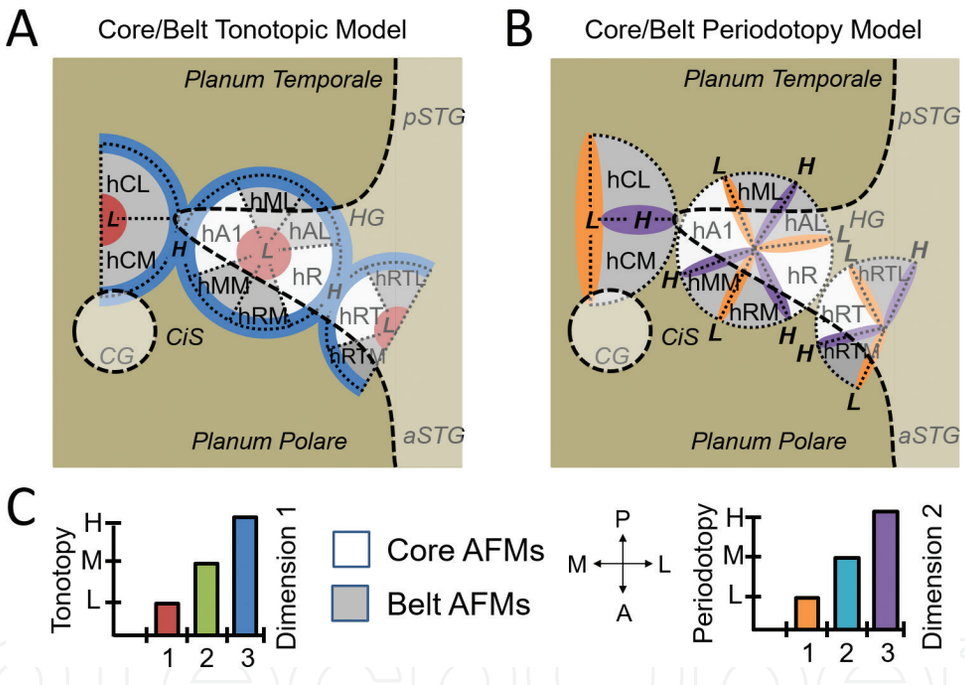

Figure 10. Diagrams of auditory field map cloverleaf clusters overlapping Heschl's gyrus. (A, B) Approximate locations of core AFMs (hA1, hR, hRT) are shown in white, and belt AFMs (hML, hAL, hRTL, hRTM, hRM, hMM, hCM, hCL) are shown in gray, as defined by [4]. Schematics were created from individual-subject data drawn from multiple phase-encoded fMRI experiments. Diagrams are oriented along the same global anatomical axes. Darker beige background indicates the plane of the lateral sulcus, while lighter beige overlay indicates gyri. The edges of gyri are also noted with dashed black lines. HG: Heschl's gyrus. a/p STG: anterior/posterior superior temporal gyrus; CiS: circular sulcus; CG: circular gyrus. **(A)** Diagram depicts the locations of tonotopic representations overlaid along the core (white) and belt (gray) AFMs. The approximate locations of low (L) and high (H) tonotopic representations are shown in red and blue, respectively. Dotted black lines mark the boundaries between AFMs within these three cloverleaf clusters: hCM/hCL cluster (partial cluster defined to date); HG cluster with hA1; hRTM/hRT/hRTL cluster (partial cluster defined to date). **(B)** Diagram now shows periodotopic representations overlaid along the same example region of cortex. L and H now refer to the approximate locations of low (orange) or high (purple) periodotopic representations, respectively. **(C)** Color legends for tonotopy schematic (*left*), core/belt AFMs (*middle left*), and periodotopy schematic (*right*). Inset legend (*middle right*) shows anatomical directions for both diagrams. M: Medial; L: lateral; A: anterior; P: posterior. For a detailed review, see [8].

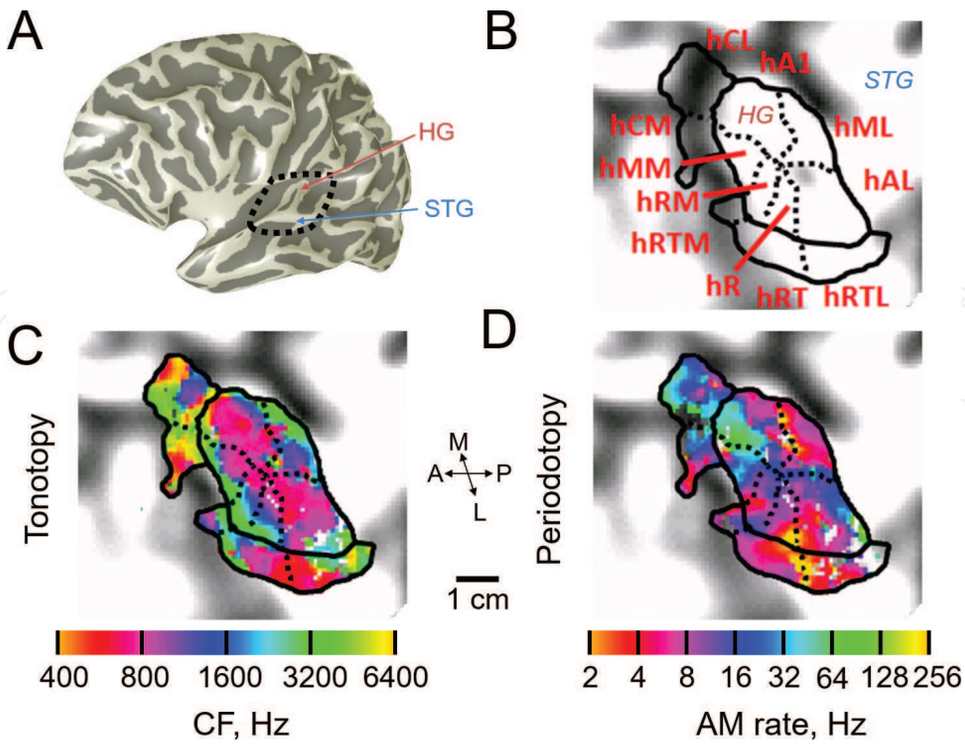

Figure 11. Example auditory field map cloverleaf cluster data in human cortex. **(A)** Inflated 3-D rendering of an individual left hemisphere cortical surface. Light gray indicates gyri; dark gray indicates sulci. HG: Heschl's gyrus, blue; STG: superior temporal gyrus, red. Black dotted line indicates HG and surrounding regions presented in **(B-D)**. **(B)** Flattened cortical surface of HG and surrounding regions. Solid black lines indicate AFM boundaries between maps along tonotopic reversals, which separate cloverleaf clusters from one another. Dotted black lines indicate AFM boundaries along periodotopic reversals between maps within a cloverleaf cluster. Red text indicates AFM names. **(C)** Tonotopic gradients measured using narrowband noise stimuli with a phase-encoded fMRI paradigm. Color overlay indicates the preferred frequency range for each voxel. CF: Center frequency in Hz. For clarity, only voxels within the core and belt AFMs are shown. Coherence ≥0.20. **(D)** Periodotopic representations measured using broadband noise stimuli with a phase-encoded fMRI paradigm. Color overlay is shown on the same flattened cortical surface as in **(C)** and now indicates the preferred period range for each voxel. AM rate: amplitude modulation rate in Hz. Other details are as in **(C)**. Inset scale bar denotes 1 cm along the flattened cortical surfaces. Inset legend shows anatomical directions for both datasets. M: Medial; L: lateral; A: anterior; P: posterior. Adapted from [4].

begin to investigate the specific functions subserved by each AFM. Based on emerging data, we also expect that neighboring cortex like planum temporale (PT) and STG will also contain AFMs organized into cloverleaf clusters.

6. Considerations for defining additional CFMs and cloverleaf clusters

To date, cloverleaf clusters have been shown to both be common to multiple sensory systems across human cortex and conserved across some primate species [2, 7, 9, 10, 20, 134, 143]. As we continue to delineate additional CFM clusters and study their functional responses, it is important to consider what homologies may exist across sensory domains and species as well as potential ways CFMs may be altering under evolutionary pressures. Evolution is an

ongoing process; CFMs and clusters are not necessarily, and in fact are unlikely to be, at an optimal evolutionary endpoint. Thus it is important to keep in mind that the cortical sensory representations that we are measuring may not be perfectly organized. In addition, with 25 million years of divergent evolution between humans and macaque monkeys, some CFMs and clusters may be unique to one species or the other [144].

Figure 12 depicts several ways in which CFMs may have changed or be in the process of changing across species or sensory domains (for extended discussion, see [5]). The size of a CFM itself (**Figure 12B**) or the total number of CFMs devoted to a particular sensory processing pathway (**Figure 12D**) may increase or decrease, reflecting an expansion or reduction of the

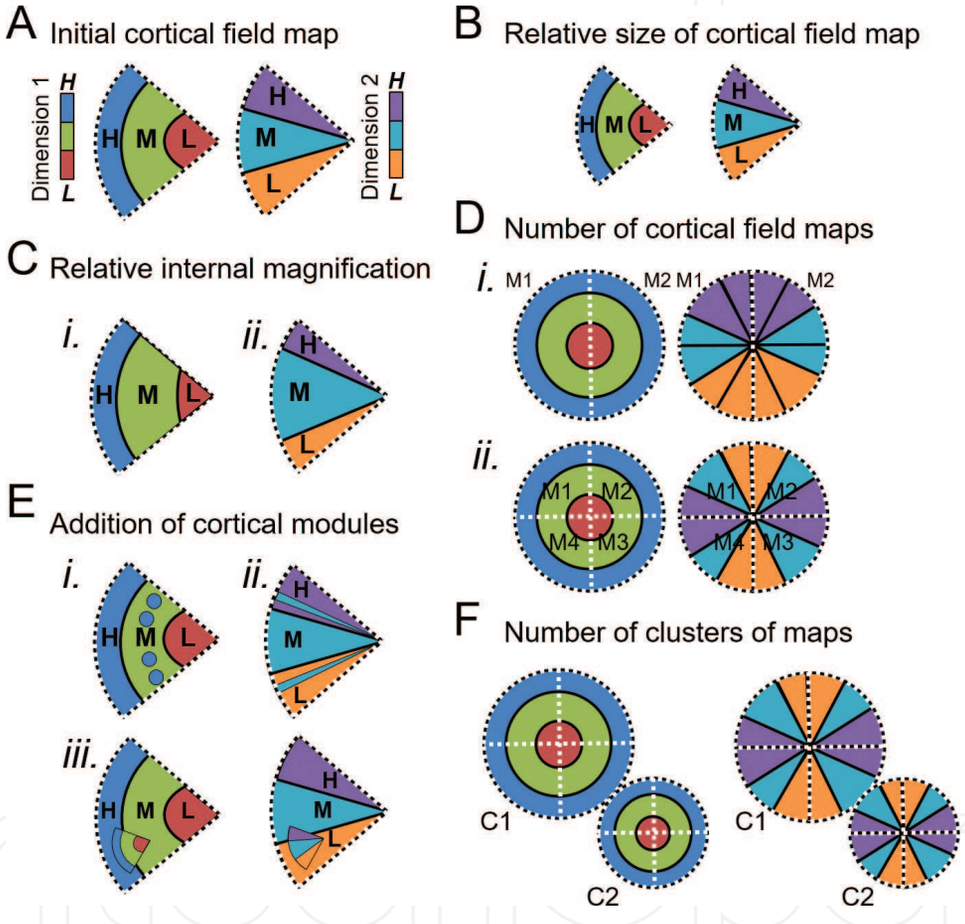

Figure 12. Potential cortical field map changes over evolution. Schematic diagrams depict numerous ways CFMs might change over the course of evolution. Consideration of such changes is important for evaluating potential homology of CFMs across sensory cortices and among species (for extended discussion, see [5]). **(A)** Each schematic shows two pictures of the same CFM, one for each orthogonal dimension (e.g., dimension 1: tonotopy or eccentricity; dimension 2: periodotopy or polar angle). The subsequent schematics depict changes to this CFM. **(B)** Overall size of CFM may be reduced. **(C)** The magnification of a particular part of the internal representations may increase for dimension 1 (*i*) and/or dimension 2 (*ii*). **(D)** The number of CFMs for a particular computation may increase or decrease (e.g., (*i*) two CFMS; (*ii*) four CFMs). **(E)** Additional representations may be in the process of emerging or combining within a complete CFM. (*i*) Additional segments of H (high; blue) representations of dimension 1 are present within the M (medium; green) representations. (*ii*) Additional segments of M (medium; teal) representations of dimension 2 are present within the H (high; purple) and L (low; orange) representations. (*iii*) A smaller complete CFM exists within the larger CFM. **(F)** New clusters of maps may emerge in neighboring regions.

importance of the particular behavior this cortex subserves. The internal structure of a CFM may be altered in the magnification of specific sections of the representations (**Figure 12C**) or may contain additional, emerging representation subsections (**Figure 12E**). Similarly, the number of cloverleaf clusters may be modified. Thus the homology of CFMs across species is very important for understanding functional similarities in different model systems, but care must also be taken to recognize what differences may exist.

In addition to the likely role of cloverleaf clusters in efficiently grouping together neurons performing associated computations, the emergence of new cloverleaf clusters during evolution as an organizational unit across cortex could facilitate the development of expanded or even novel cortical computations for an emerging species [8, 145]. In other words, once a particular organizational unit such as the cloverleaf cluster has arisen in one sensory modality, the same organizational unit might be duplicated and repeated across the brain as it evolves, following consistent genetic mechanisms during development [145]. Now that CFMs and cloverleaf clusters have been established as fundamental organizational principles in visual and auditory cortex, we can use this knowledge to guide measurements of similar topographic groupings in other sensory domains (e.g., somatosenstaion, pain matrix, olfaction; [3, 4, 146]).

7. Conclusion

Human visual and auditory cortex thus interestingly share a common organizational scheme, with each sensory system compartmentalized into CFMs that are themselves arranged on a larger scale into cloverleaf clusters. This fundamental organization provides a basic framework for the complex processing and analysis of input from sensory receptors. Such similarity may be common across many sensory domains, which may aid in the future identification of CFMs in the representation of other senses and in homologous regions in related species. The detailed examination of these CFMs and clusters in individual subjects can also be applied to the careful analysis of the computational stages of sensory processing and to the detailed tracking of cortical changes in a variety of diseases.

Acknowledgements

This material is based upon work supported by the National Science Foundation under Grant Number 1329255 and by startup funds from the Department of Cognitive Sciences at the University of California, Irvine.

Conflict of interest

The authors declare that this research was conducted in the absence of any commercial or financial relationships that could be interpreted to be a potential conflict of interest.

Author details

Alyssa A. Brewer[1,2]* and Brian Barton[1]

*Address all correspondence to: aabrewer@uci.edu

1 Department of Cognitive Sciences, University of California, Irvine, CA, USA

2 Department of Language Science, University of California, Irvine, CA, USA

References

[1] Kaas JH. Topographic maps are fundamental to sensory processing. Brain Research Bulletin. 1997;**44**(2):107-112

[2] Wandell BA, Brewer AA, Dougherty RF. Visual field map clusters in human cortex. Philosophical Transactions of the Royal Society of London. Series B, Biological Sciences. 2005;**360**(1456):693-707. DOI: 10.1098/rstb.2005.1628

[3] Sanchez-Panchuelo RM, Francis S, Bowtell R, Schluppeck D. Mapping human somatosensory cortex in individual subjects with 7T functional MRI. Journal of Neurophysiology. 2010;**103**(5):2544-2556. DOI: 10.1152/jn.01017.2009

[4] Barton B, Venezia JH, Saberi K, Hickok G, Brewer AA. Orthogonal acoustic dimensions define auditory field maps in human cortex. Proceedings of National Academy of Science U S A. 2012;**109**(50):20738-20743. DOI: 10.1073/pnas.1213381109

[5] Krubitzer LA, Seelke AM. Cortical evolution in mammals: The bane and beauty of phenotypic variability. Proceedings of the National Academy of Sciences. 2012;**109** (Supplement 1):10647-10654

[6] Van Essen DC. Organization of Visual Areas in macaque and human cerebral cortex. In: Chalupa LM, Werner JS, editors. The Visual Neurosciences. Boston: Bradford Books; 2003. pp. 507-521

[7] Brewer AA, Barton B. Visual field map organization in human visual cortex. In: Molotchnikoff S, Rouat J, editors. Visual Cortex - Current Status and Perspectives. Rijeka, Croatia: InTech; 2012. pp. 29-60. DOI: 10.5772/51914

[8] Brewer AA, Barton B. Maps of the auditory cortex. Annual Review of Neuroscience. 2016;**39**:385-407. DOI: 10.1146/annurev-neuro-070815-014045

[9] Kolster H, Mandeville JB, Arsenault JT, Ekstrom LB, Wald LL, Vanduffel W. Visual field map clusters in macaque extrastriate visual cortex. The Journal of Neuroscience. 2009;**29**(21):7031-7039. DOI: 10.1523/JNEUROSCI.0518-09.2009

[10] Kolster H, Peeters R, Orban GA. The retinotopic organization of the human middle temporal area MT/V5 and its cortical neighbors. The Journal of Neuroscience. 2010;**30**(29):9801-9820. DOI: 10.1523/JNEUROSCI.2069-10.2010

[11] Barton B, Brewer AA. Visual field map clusters in high-order visual processing: Organization of V3A/V3B and a new cloverleaf cluster in the posterior superior temporal sulcus. Frontiers in Integrative Neuroscience. 2017;**11**:4. DOI: 10.3389/fnint.2017.00004

[12] Wandell BA, Dumoulin SO, Brewer AA. Visual field maps in human cortex. Neuron. 2007;**56**(2):366-383. DOI: 10.1016/j.neuron.2007.10.012

[13] Press WA, Brewer AA, Dougherty RF, Wade AR, Wandell BA. Visual areas and spatial summation in human visual cortex. Vision Research. 2001;**41**(10-11):1321-1332

[14] Mitchison G. Neuronal branching patterns and the economy of cortical wiring. Proceedings: Biological Sciences. 1991;**245**(1313):151-158. DOI: 10.1098/rspb.1991.0102

[15] Chklovskii DB, Koulakov AA. Maps in the brain: What can we learn from them? Annual Review of Neuroscience. 2004;**27**:369-392. DOI: 10.1146/annurev.neuro.27.070203.144226

[16] Shapley R, Hawken M, Xing D. The dynamics of visual responses in the primary visual cortex. Progress in Brain Research. 2007;**165**:21-32. DOI: 10.1016/S0079-6123(06)65003-6

[17] Moradi F, Heeger DJ. Inter-ocular contrast normalization in human visual cortex. Journal of Vision. 2009;**9**(3):13 1-13 1322. DOI: 10.1167/9.3.13

[18] Braitenberg V, Schüz A. Cortex: Statistics and Geometry of Neuronal Connectivity. 2nd ed. 1998

[19] Arcaro MJ, McMains SA, Singer BD, Kastner S. Retinotopic organization of human ventral visual cortex. The Journal of Neuroscience. 2009;**29**(34):10638-10652. DOI: 10.1523/JNEUROSCI.2807-09.2009

[20] Brewer AA, Liu J, Wade AR, Wandell BA. Visual field maps and stimulus selectivity in human ventral occipital cortex. Nature Neuroscience. 2005;**8**(8):1102-1109. DOI: 10.1038/nn1507

[21] Baseler HA, Brewer AA, Sharpe LT, Morland AB, Jagle H, Wandell BA. Reorganization of human cortical maps caused by inherited photoreceptor abnormalities. Nature Neuroscience. 2002;**5**(4):364-370. DOI: 10.1038/nn817

[22] Hoffmann MB, Tolhurst DJ, Moore AT, Morland AB. Organization of the visual cortex in human albinism. The Journal of Neuroscience. 2003;**23**(26):8921-8930

[23] Hoffmann MB, Kaule FR, Levin N, Masuda Y, Kumar A, Gottlob I, et al. Plasticity and stability of the visual system in human achiasma. Neuron. 2012;**75**(3):393-401. DOI: 10.1016/j.neuron.2012.05.026

[24] Baseler HA, Gouws A, Haak KV, Racey C, Crossland MD, Tufail A, et al. Large-scale remapping of visual cortex is absent in adult humans with macular degeneration. Nature Neuroscience. 2011;**14**(5):649-655. DOI: 10.1038/nn.2793

[25] Fine I, Wade AR, Brewer AA, May MG, Goodman DF, Boynton GM, et al. Long-term deprivation affects visual perception and cortex. Nature Neuroscience. 2003;**6**(9):915-916. DOI: 10.1038/nn1102

[26] Muckli L, Naumer MJ, Singer W. Bilateral visual field maps in a patient with only one hemisphere. Proceedings of National Academy of Sciences U S A. 2009;**106**(31):13034-13039. DOI: 10.1073/pnas.0809688106

[27] Brewer AA, Barton B. Visual cortex in aging and Alzheimer's disease: Changes in visual field maps and population receptive fields. Frontiers in Psychology. 2014;**5**:74. DOI: 10.3389/fpsyg.2014.00074

[28] Brewer AA, Barton B. Changes in visual cortex in healthy aging and dementia. In: Moretti DV, editor. Update on Dementia. Rijeka, Croatia: InTech; 2016. pp. 273-310. DOI: 10.5772/61983

[29] DeYoe EA, Carman GJ, Bandettini P, Glickman S, Wieser J, Cox R, et al. Mapping striate and extrastriate visual areas in human cerebral cortex. Proceedings of National Academy of Sciences (USA). 1996;**93**:2382-2386

[30] Engel SA, Glover GH, Wandell BA. Retinotopic organization in human visual cortex and the spatial precision of functional MRI. Cerebral Cortex. 1997;**7**(2):181-192

[31] Engel SA, Rumelhart DE, Wandell BA, Lee AT, Glover GH, Chichilnisky EJ, et al. fMRI of human visual cortex. Nature. 1994;**369**(6481):525. DOI: 10.1038/369525a0

[32] Sereno MI, Dale AM, Reppas JB, Kwong KK, Belliveau JW, Brady TJ, et al. Borders of multiple visual areas in humans revealed by functional magnetic resonance imaging. Science. 1995;**268**(5212):889-893

[33] Humphries C, Liebenthal E, Binder JR. Tonotopic organization of human auditory cortex. NeuroImage. 2010;**50**(3):1202-1211. DOI: 10.1016/j.neuroimage.2010.01.046

[34] Talavage TM, Sereno MI, Melcher JR, Ledden PJ, Rosen BR, Dale AM. Tonotopic organization in human auditory cortex revealed by progressions of frequency sensitivity. Journal of Neurophysiology. 2004;**91**(3):1282-1296. DOI: 10.1152/jn.01125.2002

[35] Petkov CI, Kayser C, Augath M, Logothetis NK. Optimizing the imaging of the monkey auditory cortex: Sparse vs. continuous fMRI. Magnetic Resonance Imaging. 2009;**27**(8):1065-1073. DOI: 10.1016/j.mri.2009.01.018

[36] Joly O, Baumann S, Balezeau F, Thiele A, Griffiths TD. Merging functional and structural properties of the monkey auditory cortex. Frontiers in Neuroscience. 2014;**8**:198. DOI: 10.3389/fnins.2014.00198

[37] Bandettini PA, Jesmanowicz A, Van Kylen J, Birn RM, Hyde JS. Functional MRI of brain activation induced by scanner acoustic noise. Magnetic Resonance in Medicine. 1998;**39**(3):410-416

[38] Gaab N, Gabrieli JD, Glover GH. Assessing the influence of scanner background noise on auditory processing. II. An fMRI study comparing auditory processing in the absence and presence of recorded scanner noise using a sparse design. Human Brain Mapping. 2007;**28**(8):721-732. DOI: 10.1002/hbm.20299

[39] Scarff CJ, Dort JC, Eggermont JJ, Goodyear BG. The effect of MR scanner noise on auditory cortex activity using fMRI. Human Brain Mapping. 2004;**22**(4):341-349. DOI: 10.1002/hbm.20043

[40] Clarke S, Morosan P. Architecture, connectivity, and transmitter receptors of human auditory cortex. In: Poeppel D, Overath T, Popper A, Richard R, editors. The Human Auditory Cortex. New York: Springer; 2012. pp. 11-38

[41] Dougherty RF, Koch VM, Brewer AA, Fischer B, Modersitzki J, Wandell BA. Visual field representations and locations of visual areas V1/2/3 in human visual cortex. Journal of Vision. 2003;**3**(10):586-598. DOI: 10:1167/3.10.1

[42] Galaburda A, Sanides F. Cytoarchitectonic organization of the human auditory cortex. The Journal of Comparative Neurology. 1980;**190**(3):597-610. DOI: 10.1002/cne.901900312

[43] Morosan P, Rademacher J, Schleicher A, Amunts K, Schormann T, Zilles K. Human primary auditory cortex: Cytoarchitectonic subdivisions and mapping into a spatial reference system. NeuroImage. 2001;**13**(4):684-701. DOI: 10.1006/nimg.2000.0715

[44] Rademacher J, Caviness VS Jr, Steinmetz H, Galaburda AM. Topographical variation of the human primary cortices: Implications for neuroimaging, brain mapping, and neurobiology. Cerebral Cortex. 1993;**3**(4):313-329

[45] Rademacher J, Morosan P, Schormann T, Schleicher A, Werner C, Freund HJ, et al. Probabilistic mapping and volume measurement of human primary auditory cortex. NeuroImage. 2001;**13**(4):669-683. DOI: 10.1006/nimg.2000.0714

[46] Talairach J, Tournoux P. Col-Planar Stereotax Atlas of the Human Brain. New York: Thieme Medical Publishers; 1988

[47] Collins DL, Neelin P, Peters TM, Evans AC. Automatic 3D intersubject registration of MR volumetric data in standardized Talairach space. Journal of Computer Assisted Tomography. 1994;**18**(2):192-205

[48] Dumoulin SO, Wandell BA. Population receptive field estimates in human visual cortex. NeuroImage. 2008;**39**(2):647-660. DOI: 10.1016/j.neuroimage.2007.09.034

[49] Hoffmann MB, Seufert PS, Schmidtborn LC. Perceptual relevance of abnormal visual field representations: Static visual field perimetry in human albinism. The British Journal of Ophthalmology. 2007;**91**(4):509-513. DOI: 10.1136/bjo.2006.094854

[50] Santoro R, Moerel M, De Martino F, Valente G, Ugurbil K, Yacoub E, et al. Reconstructing the spectrotemporal modulations of real-life sounds from fMRI response patterns. Proceedings of National Academy of Sciences USA. 2017;**114**(18):4799-4804. DOI: 10.1073/pnas.1617622114

[51] Wade AR, Brewer AA, Rieger JW, Wandell BA. Functional measurements of human ventral occipital cortex: Retinotopy and colour. Philosophical Transactions of the Royal Society of London. Series B, Biological Sciences. 2002;**357**(1424):963-973. DOI: 10.1098/rstb.2002.1108

[52] Tyler CW, Wade AR. Extended concepts of occipital retinotopy. Current Medical Imaging Review. 2005;**1**:3190329

[53] Hart HC, Hall DA, Palmer AR. The sound-level-dependent growth in the extent of fMRI activation in Heschl's gyrus is different for low- and high-frequency tones. Hearing Research. 2003;**179**(1-2):104-112

[54] Logothetis NK, Wandell BA. Interpreting the BOLD signal. Annual Review of Physiology. 2004;**66**:735-769. DOI: 10.1146/annurev.physiol.66.082602.092845

[55] Menon RS, Kim SG. Spatial and temporal limits in cognitive neuroimaging with fMRI. Trends in Cognitive Sciences. 1999;**3**(6):207-216

[56] Tanji K, Leopold DA, Ye FQ, Zhu C, Malloy M, Saunders RC, et al. Effect of sound intensity on tonotopic fMRI maps in the unanesthetized monkey. NeuroImage. 2010;**49**(1):150-157. DOI: 10.1016/j.neuroimage.2009.07.029

[57] Amunts K, Schleicher A, Burgel U, Mohlberg H, Uylings HB, Zilles K. Broca's region revisited: Cytoarchitecture and intersubject variability. The Journal of Comparative Neurology. 1999;**412**(2):319-341

[58] Leonard CM, Puranik C, Kuldau JM, Lombardino LJ. Normal variation in the frequency and location of human auditory cortex landmarks. Heschl's gyrus: Where is it? Cerebral Cortex. 1998;**8**(5):397-406

[59] Brewer AA, Barton B. Developmental plasticity: FMRI investigations into human visual cortex. In: Papageorgiou TD, Christopoulos G, Smirnakis S, editors. Advanced Brain Neuroimaging Topics in Health and Disease - Methods and Applications. Rijeka, Croatia: InTech; 2014. pp. 305-334. DOI: 10.5772/58256

[60] Brewer AA. Visual maps: To merge or not to merge. Current Biology. 2009;**19**(20): R945-R947. DOI: 10.1016/j.cub.2009.09.016

[61] Katz LC, Shatz CJ. Synaptic activity and the construction of cortical circuits. Science. 1996;**274**(5290):1133-1138

[62] Polleux F, Ince-Dunn G, Ghosh A. Transcriptional regulation of vertebrate axon guidance and synapse formation. Nature Reviews. Neuroscience. 2007;**8**(5):331-340. DOI: 10.1038/nrn2118

[63] Bartels A, Zeki S. The architecture of the colour Centre in the human visual brain: New results and a review. The European Journal of Neuroscience. 2000;**12**(1):172-193

[64] Van Essen DC. In: Chalupa L, Werner J, editors. Organization of Visual Areas in Macaque and Human Cerebral Cortex. Boston: Bradford; 2003

[65] Lehky SR, Sereno AB. Population coding of visual space: Modeling. Frontiers in Computational Neuroscience. 2011;**4**:155. DOI: 10.3389/fncom.2010.00155

[66] Haak KV, Winawer J, Harvey BM, Renken R, Dumoulin SO, Wandell BA, et al. Connective field modeling. NeuroImage. 2012;**66C**:376-384. DOI: 10.1016/j.neuroimage.2012.10.037

[67] DiCarlo JJ, Maunsell JH. Anterior inferotemporal neurons of monkeys engaged in object recognition can be highly sensitive to object retinal position. Journal of Neurophysiology. 2003;**89**(6):3264-3278. DOI: 10.1152/jn.00358.2002

[68] Lehky SR, Sereno ME, Sereno AB. Characteristics of eye-position gain field populations determine geometry of visual space. Frontiers in Integrative Neuroscience. 2015;**9**:72. DOI: 10.3389/fnint.2015.00072

[69] Hagler DJ Jr, Riecke L, Sereno MI. Parietal and superior frontal visuospatial maps activated by pointing and saccades. NeuroImage. 2007;**35**(4):1562-1577. DOI: 10.1016/j.neuroimage.2007.01.033

[70] Kastner S, DeSimone K, Konen CS, Szczepanski SM, Weiner KS, Schneider KA. Topographic maps in human frontal cortex revealed in memory-guided saccade and spatial working-memory tasks. Journal of Neurophysiology. 2007;**97**(5):3494-3507. DOI: 10.1152/jn.00010.2007

[71] Konen CS, Kastner S. Representation of eye movements and stimulus motion in topographically organized areas of human posterior parietal cortex. The Journal of Neuroscience. 2008;**28**(33):8361-8375. DOI: 10.1523/JNEUROSCI.1930-08.2008

[72] Swisher JD, Halko MA, Merabet LB, McMains SA, Somers DC. Visual topography of human intraparietal sulcus. The Journal of Neuroscience. 2007;**27**(20):5326-5337. DOI: 10.1523/JNEUROSCI.0991-07.2007

[73] Hagler DJ Jr, Sereno MI. Spatial maps in frontal and prefrontal cortex. NeuroImage 2006;**29**(2):567-577. DOI: 10.1016/j.neuroimage.2005.08.058

[74] Sereno MI, Pitzalis S, Martinez A. Mapping of contralateral space in retinotopic coordinates by a parietal cortical area in humans. Science. 2001;**294**(5545):1350-1354. DOI: 10.1126/science.1063695

[75] Sereno MI, Huang RS. A human parietal face area contains aligned head-centered visual and tactile maps. Nature Neuroscience. 2006;**9**(10):1337-1343. DOI: 10.1038/nn1777

[76] Silver MA, Kastner S. Topographic maps in human frontal and parietal cortex. Trends in Cognitive Sciences. 2009;**13**(11):488-495. DOI: 10.1016/j.tics.2009.08.005

[77] Silver MA, Ress D, Heeger DJ. Topographic maps of visual spatial attention in human parietal cortex. Journal of Neurophysiology. 2005;**94**(2):1358-1371. DOI: 10.1152/jn.01316.2004

[78] Saygin AP, Sereno MI. Retinotopy and attention in human occipital, temporal, parietal, and frontal cortex. Cerebral Cortex. 2008;**18**(9):2158-2168. DOI: 10.1093/cercor/bhm242

[79] Szczepanski SM, Konen CS, Kastner S. Mechanisms of spatial attention control in frontal and parietal cortex. The Journal of Neuroscience. 2010;**30**(1):148-160. DOI: 10.1523/JNEUROSCI.3862-09.2010

[80] Lauritzen TZ, D'Esposito M, Heeger DJ, Silver MA. Top-down flow of visual spatial attention signals from parietal to occipital cortex. Journal of Vision. 2009;**9**(13):181-184. DOI: 10.1167/9.13.18

[81] Larsson J, Heeger DJ. Two retinotopic visual areas in human lateral occipital cortex. The Journal of Neuroscience. 2006;**26**(51):13128-13142. DOI: 10.1523/JNEUROSCI.1657-06.2006

[82] Langner G, Albert M, Briede T. Temporal and spatial coding of periodicity information in the inferior colliculus of awake chinchilla (Chinchilla laniger). Hearing Research. 2002;**168**(1-2):110-130

[83] Adams DL, Sincich LC, Horton JC. Complete pattern of ocular dominance columns in human primary visual cortex. The Journal of Neuroscience. 2007;**27**(39):10391-10403. DOI: 10.1523/JNEUROSCI.2923-07.2007

[84] Bartfeld E, Grinvald A. Relationships between orientation-preference pinwheels, cytochrome oxidase blobs, and ocular-dominance columns in primate striate cortex. Proceedings of National Academy of Sciences U S A. 1992;**89**(24):11905-11909

[85] Livingstone MS, Hubel DH. Anatomy and physiology of a color system in the primate visual cortex. The Journal of Neuroscience. 1984;**4**(1):309-356

[86] Schira MM, Tyler CW, Breakspear M, Spehar B. The foveal confluence in human visual cortex. The Journal of Neuroscience. 2009;**29**(28):9050-9058. DOI: 10.1523/JNEUROSCI.1760-09.2009

[87] Schira MM, Tyler CW, Spehar B, Breakspear M. Modeling magnification and anisotropy in the primate foveal confluence. PLoS Computational Biology. 2010;**6**(1). DOI: 10.1371/journal.pcbi.1000651

[88] Hasson U, Hendler T, Ben Bashat D, Malach R. Vase or face? A neural correlate of shape-selective grouping processes in the human brain. Journal of Cognitive Neuroscience. 2001;**13**(6):744-753. DOI: 10.1162/08989290152541412

[89] Malach R, Levy I, Hasson U. The topography of high-order human object areas. Trends in Cognitive Sciences. 2002;**6**(4):176-184

[90] Tootell RB, Hadjikhani N. Where is 'dorsal V4' in human visual cortex? Retinotopic, topographic and functional evidence. Cerebral Cortex. 2001;**11**(4):298-311

[91] Larsson J, Landy MS, Heeger DJ. Orientation-selective adaptation to first- and second-order patterns in human visual cortex. Journal of Neurophysiology. 2006;**95**(2):862-881. DOI: 10.1152/jn.00668.2005

[92] Sayres R, Grill-Spector K. Relating retinotopic and object-selective responses in human lateral occipital cortex. Journal of Neurophysiology. 2008;**100**(1):249-267. DOI: 10.1152/jn.01383.2007

[93] McKyton A, Zohary E. Beyond retinotopic mapping: The spatial representation of objects in the human lateral occipital complex. Cerebral Cortex. 2007;**17**(5):1164-1172. DOI: 10.1093/cercor/bhl027

[94] Hemond CC, Kanwisher NG, Op de Beeck HP. A preference for contralateral stimuli in human object- and face-selective cortex. PLoS One. 2007;**2**(6):e574. DOI: 10.1371/journal.pone.0000574

[95] Niemeier M, Goltz HC, Kuchinad A, Tweed DB, Vilis T. A contralateral preference in the lateral occipital area: Sensory and attentional mechanisms. Cerebral Cortex. 2005;**15**(3):325-331. DOI: 10.1093/cercor/bhh134

[96] Huk AC, Dougherty RF, Heeger DJ. Retinotopy and functional subdivision of human areas MT and MST. The Journal of Neuroscience. 2002;**22**(16):7195-7205. DOI: 20026661

[97] Amano K, Wandell BA, Dumoulin SO. Visual field maps, population receptive field sizes, and visual field coverage in the human MT+ complex. Journal of Neurophysiology. 2009;**102**(5):2704-2718. DOI: 10.1152/jn.00102.2009

[98] Newsome WT, Mikami A, Wurtz RH. Motion selectivity in macaque visual cortex. III. Psychophysics and physiology of apparent motion. Journal of Neurophysiology. 1986;**55**(6):1340-1351. DOI: 10.1152/jn.1986.55.6.1340

[99] Hedges JH, Gartshteyn Y, Kohn A, Rust NC, Shadlen MN, Newsome WT, et al. Dissociation of neuronal and psychophysical responses to local and global motion. Current Biology. 2011;**21**(23):2023-2028. DOI: 10.1016/j.cub.2011.10.049

[100] Hoffman EA, Haxby JV. Distinct representations of eye gaze and identity in the distributed human neural system for face perception. Nature Neuroscience. 2000;**3**(1):80-84. DOI: 10.1038/71152

[101] Gilaie-Dotan S, Kanai R, Bahrami B, Rees G, Saygin AP. Neuroanatomical correlates of biological motion detection. Neuropsychologia. 2013;**51**(3):457-463. DOI: 10.1016/j.neuropsychologia.2012.11.027

[102] Beauchamp MS, Lee KE, Argall BD, Martin A. Integration of auditory and visual information about objects in superior temporal sulcus. Neuron. 2004;**41**(5):809-823

[103] Zhu LL, Beauchamp MS. Mouth and voice: A relationship between visual and auditory preference in the human superior temporal sulcus. The Journal of Neuroscience. 2017;**37**(10):2697-2708. DOI: 10.1523/JNEUROSCI.2914-16.2017

[104] Smith AT, Greenlee MW, Singh KD, Kraemer FM, Hennig J. The processing of first- and second-order motion in human visual cortex assessed by functional magnetic resonance imaging (fMRI). The Journal of Neuroscience. 1998;**18**(10):3816-3830

[105] Smith AT, Singh KD, Williams AL, Greenlee MW. Estimating receptive field size from fMRI data in human striate and extrastriate visual cortex. Cerebral Cortex. 2001; **11**(12):1182-1190

[106] Tootell RB, Hadjikhani N, Hall EK, Marrett S, Vanduffel W, Vaughan JT, et al. The retinotopy of visual spatial attention. Neuron. 1998;**21**(6):1409-1422

[107] Tootell RB, Mendola JD, Hadjikhani NK, Ledden PJ, Liu AK, Reppas JB, et al. Functional analysis of V3A and related areas in human visual cortex. The Journal of Neuroscience. 1997;**17**(18):7060-7078

[108] Schluppeck D, Glimcher P, Heeger DJ. Topographic organization for delayed saccades in human posterior parietal cortex. Journal of Neurophysiology. 2005;**94**(2):1372-1384. DOI: 10.1152/jn.01290.2004

[109] Pitzalis S, Galletti C, Huang RS, Patria F, Committeri G, Galati G, et al. Wide-field retinotopy defines human cortical visual area v6. The Journal of Neuroscience. 2006;**26**(30):7962-7973. DOI: 10.1523/JNEUROSCI.0178-06.2006

[110] Pitzalis S, Sereno MI, Committeri G, Fattori P, Galati G, Patria F, et al. Human v6: The medial motion area. Cerebral Cortex. 2010;**20**(2):411-424. DOI: 10.1093/cercor/bhp112

[111] Ress D, Chandrasekaran B. Tonotopic organization in the depth of human inferior colliculus. Frontiers in Human Neuroscience. 2013;**7**:586. DOI: 10.3389/fnhum.2013.00586

[112] Chang KH, Thomas JM, Boynton GM, Fine I. Reconstructing tone sequences from functional magnetic resonance imaging blood-oxygen level dependent responses within human primary auditory cortex. Frontiers in Psychology. 2017;**8**:1983. DOI: 10.3389/fpsyg.2017.01983

[113] Wessinger CM, VanMeter J, Tian B, Van Lare J, Pekar J, Rauschecker JP. Hierarchical organization of the human auditory cortex revealed by functional magnetic resonance imaging. Journal of Cognitive Neuroscience. 2001;**13**(1):1-7

[114] Langner G, Sams M, Heil P, Schulze H. Frequency and periodicity are represented in orthogonal maps in the human auditory cortex: Evidence from magnetoencephalography. Journal of Comparative Physiology. A. 1997;**181**(6):665-676

[115] Baumann S, Griffiths TD, Sun L, Petkov CI, Thiele A, Rees A. Orthogonal representation of sound dimensions in the primate midbrain. Nature Neuroscience. 2011;**14**(4):423-425. DOI: 10.1038/nn.2771

[116] Langner G, Schreiner CE. Periodicity coding in the inferior colliculus of the cat. I. Neuronal mechanisms. Journal of Neurophysiology. 1988;**60**(6):1799-1822

[117] Merzenich MM, Brugge JF. Representation of the cochlear partition of the superior temporal plane of the macaque monkey. Brain Research. 1973;**50**(2):275-296

[118] Galaburda AM, Pandya DN. The intrinsic architectonic and connectional organization of the superior temporal region of the rhesus monkey. The Journal of Comparative Neurology. 1983;**221**(2):169-184. DOI: 10.1002/cne.902210206

[119] Fullerton BC, Pandya DN. Architectonic analysis of the auditory-related areas of the superior temporal region in human brain. The Journal of Comparative Neurology. 2007;**504**(5):470-498. DOI: 10.1002/cne.21432

[120] Sweet RA, Dorph-Petersen KA, Lewis DA. Mapping auditory core, lateral belt, and parabelt cortices in the human superior temporal gyrus. The Journal of Comparative Neurology. 2005;**491**(3):270-289. DOI: 10.1002/cne.20702

[121] Dick F, Tierney AT, Lutti A, Josephs O, Sereno MI, Weiskopf N. In vivo functional and myeloarchitectonic mapping of human primary auditory areas. The Journal of Neuroscience. 2012;**32**(46):16095-16105

[122] Kaas JH, Hackett TA. Subdivisions of auditory cortex and levels of processing in primates. Audiology & Neuro-Otology. 1998;**3**(2-3):73-85

[123] Kaas JH, Hackett TA. Subdivisions of auditory cortex and processing streams in primates. Proceedings of National Academy of Sciences U S A. 2000;**97**(22):11793-11799. DOI: 10.1073/pnas.97.22.11793

[124] Hackett TA. Information flow in the auditory cortical network. Hearing Research. 2011;**271**(1-2):133-146. DOI: 10.1016/j.heares.2010.01.011

[125] Hackett TA, Stepniewska I, Kaas JH. Subdivisions of auditory cortex and ipsilateral cortical connections of the parabelt auditory cortex in macaque monkeys. The Journal of Comparative Neurology. 1998;**394**(4):475-495

[126] Morel A, Garraghty PE, Kaas JH. Tonotopic organization, architectonic fields, and connections of auditory cortex in macaque monkeys. The Journal of Comparative Neurology. 1993;**335**(3):437-459. DOI: 10.1002/cne.903350312

[127] Jones EG, Dell'Anna ME, Molinari M, Rausell E, Hashikawa T. Subdivisions of macaque monkey auditory cortex revealed by calcium-binding protein immunoreactivity. The Journal of Comparative Neurology. 1995;**362**(2):153-170. DOI: 10.1002/cne.903620202

[128] Molinari M, Dell'Anna ME, Rausell E, Leggio MG, Hashikawa T, Jones EG. Auditory thalamocortical pathways defined in monkeys by calcium-binding protein immunoreactivity. The Journal of Comparative Neurology. 1995;**362**(2):171-194. DOI: 10.1002/cne.903620203

[129] Kusmierek P, Rauschecker JP. Functional specialization of medial auditory belt cortex in the alert rhesus monkey. Journal of Neurophysiology. 2009;**102**(3):1606-1622. DOI: 10.1152/jn.00167.2009

[130] Rauschecker JP, Tian B, Hauser M. Processing of complex sounds in the macaque nonprimary auditory cortex. Science. 1995;**268**(5207):111-114

[131] Tian B, Rauschecker JP. Processing of frequency-modulated sounds in the lateral auditory belt cortex of the rhesus monkey. Journal of Neurophysiology. 2004;**92**(5):2993-3013. DOI: 10.1152/jn.00472.2003

[132] Kajikawa Y, Frey S, Ross D, Falchier A, Hackett TA, Schroeder CE. Auditory properties in the parabelt regions of the superior temporal gyrus in the awake macaque monkey: An initial survey. The Journal of Neuroscience. 2015;**35**(10):4140-4150. DOI: 10.1523/JNEUROSCI.3556-14.2015

[133] Hickok G, Poeppel D. The cortical organization of speech processing. Nature Reviews. Neuroscience. 2007;**8**(5):393-402. DOI: 10.1038/nrn2113

[134] Brewer AA, Barton B. Human auditory cortex. In: Hickok G, Small SL, editors. Neurobiology of Language. Cambridge: Academic Press, Elsevier; 2016. pp. 49-58. DOI: 10.1016/B978-0-12-407794-2.00005-5

[135] Dau T, Kollmeier B, Kohlrausch A. Modeling auditory processing of amplitude modulation. II. Spectral and temporal integration. The Journal of the Acoustical Society of America. 1997;**102**(5 Pt 1):2906-2919

[136] Ewert SD, Dau T. Characterizing frequency selectivity for envelope fluctuations. The Journal of the Acoustical Society of America. 2000;**108**(3 Pt 1):1181-1196

[137] Hsieh IH, Saberi K. Detection of sinusoidal amplitude modulation in logarithmic frequency sweeps across wide regions of the spectrum. Hearing Research. 2010;**262**(1-2):9-18. DOI: 10.1016/j.heares.2010.02.002

[138] Langner G, Dinse HR, Godde B. A map of periodicity orthogonal to frequency representation in the cat auditory cortex. Frontiers in Integrative Neuroscience. 2009;**3**:27. DOI: 10.3389/neuro.07.027.2009

[139] de la Mothe LA, Blumell S, Kajikawa Y, Hackett TA. Cortical connections of the auditory cortex in marmoset monkeys: Core and medial belt regions. The Journal of Comparative Neurology 2006;**496**(1):27-71. DOI: 10.1002/cne.20923

[140] Petkov CI, Kayser C, Augath M, Logothetis NK. Functional imaging reveals numerous fields in the monkey auditory cortex. PLoS Biology. 2006;**4**(7):e215. DOI: 10.1371/journal.pbio.0040215

[141] Pandya DN, Sanides F. Architectonic parcellation of the temporal operculum in rhesus monkey and its projection pattern. Zeitschrift für Anatomie und Entwicklungsgeschichte. 1973;**139**(2):127-161

[142] Kayser C, Petkov CI, Augath M, Logothetis NK. Functional imaging reveals visual modulation of specific fields in auditory cortex. The Journal of Neuroscience. 2007; **27**(8):1824-1835. DOI: 10.1523/JNEUROSCI.4737-06.2007

[143] Brewer AA, Press WA, Logothetis NK, Wandell BA. Visual areas in macaque cortex measured using functional magnetic resonance imaging. The Journal of Neuroscience. 2002;**22**(23):10416-10426

[144] Hedges S, Kumar S. Genomic clocks and evolutionary timescales. Trends in Genetics. 2003;**19**:200-206

[145] Krubitzer L. The magnificent compromise: Cortical field evolution in mammals. Neuron. 2007;**56**(2):201-208. DOI: 10.1016/j.neuron.2007.10.002

[146] Mancini F, Haggard P, Iannetti GD, Longo MR, Sereno MI. Fine-grained nociceptive maps in primary somatosensory cortex. The Journal of Neuroscience. 2012;**32**(48): 17155-17162. DOI: 10.1523/JNEUROSCI.3059-12.2012